1

A Signal Processing Outlook Toward Joint Radar-Communications

Kumar Vijay Mishra[1], M. R. Bhavani Shankar[2], Björn Ottersten[3], and A. Lee Swindlehurst[4]

[1] *United States CCDC Army Research Laboratory, Adelphi, MD, USA*
[2] *Interdisciplinary Centre for Security, Reliability and Trust (SnT), University of Luxembourg, Luxembourg*
[3] *KTH Royal Institute of Technology, Stockholm, Sweden*
[4] *University of California, Irvine, CA, USA*

1.1 Introduction

In recent years, sensing systems (radar, lidar, or sonar) that share the spectrum with wireless communications (radio-frequency/RF, optical, or acoustical) and still operate without any significant performance losses have captured significant research interest [Paul et al., 2017; Hassanien et al., 2017]. The interest in such spectrum-sharing systems is largely because the spectrum required by the wireless media is a scarce resource, while performance of both communications and remote sensing systems improves by exploiting a wider spectrum.

Several portions of frequency bands – from Very High Frequency (VHF) to Terahertz (THF) – are allocated exclusively for different radar applications [Cohen et al., 2018]. Although a large fraction of these bands remains underutilized, radars need to maintain constant access to these bands for target sensing and detection as well as obtain more spectrum to accomplish missions such as secondary surveillance, multi-function integrated RF operations, communications-enabled autonomous driving and cognitive capabilities. On the other hand, the wireless industry's demand for spectrum continues to increase for providing new services and accommodating a massive number of users with a high data rate requirement. The present spectrum is used very inefficiently due to its highly fragmented allocation. Emerging wireless systems such as commercial Long Term-Evolution (LTE) communications technology, fifth-generation (5G), Wi-Fi, Internet-of-Things (IoT), and Citizens Broadband Radio Services (CBRS) already cause spectral interference to legacy military, weather, astronomy, and aircraft surveillance radars (ASR) [Paul et al., 2017; Cohen et al., 2018]. Similarly, radar signals in adjacent bands leak to spectrum allocated for communications and deteriorate the service quality. Therefore, it is essential and beneficial for radar and communications to develop strategies to simultaneously and opportunistically operate in the same spectral bands in a mutually beneficial manner.

At the lower end of the spectrum in the VHF (30–300 MHz), Ultra High Frequency (UHF) (300–1000 MHz), and L-bands (1–2 GHz), radar systems such as FOliage PENetration (FOPEN) radar, astronomy/ionosphere radars, and Air Route Surveillance Radar (ARSR) have been encountering and managing interference from the broadcast and TV stations for decades now. The spectral congestion in centimeter-wave (cmWave) bands (S-, C-, X-, Ku-, and K-) arose later, primarily due to LTE waveforms, e.g. 802.11b/g/n (2.4 GHz) Wide-band Code Division Multiplexing Access (WCDMA), WiMAX LTE, LTE Global System for Mobile (GSM) communication, Enhanced

Signal Processing for Joint Radar Communications, First Edition.
Edited by Kumar Vijay Mishra, M. R. Bhavani Shankar, Björn Ottersten, and A. Lee Swindlehurst.

Data rates for GSM Evolution (EDGE), 802.11a/ac Very High Throughput (VHT) wireless LAN (WLAN), and commercial flight communications that now share spectrum with radars such as ASR, Terminal Weather Doppler Radar (TDWR) network, and other weather radars.

The spectral overlap of cmWave radars with a number of wireless systems at the 3.5 GHz frequency band led to the 2012 U. S. President's Council of Advisors on Science and Technology (PCAST) report on spectrum-sharing [2012], and changes in regulation for this band became a driver for spectrum-sharing research programs of multiple agencies [Cohen et al., 2018].

Today, it is the higher end of the RF spectrum, i.e., the millimeter-wave (mmWave), formally defined with the frequency range 30–300 GHz, that requires concerted efforts for spectrum management because its technologies are in an early development stage. Increasingly, the mmWave systems [Rappaport et al., 2015] are the preferred technology for near-field communications since they provide transmission bandwidth that is several GHz wide and currently unlicensed. This enables applications that require huge data rates such as 5G wireless backhaul, uncompressed high-definition (HD) video, in-room gaming, intra-large-vehicle communications, inter-vehicular communications, indoor positioning systems, and IoT-enabled wearable technologies [Daniels and Heath Jr, 2007]. There has also been a spurt of novel sensing systems in the mmWave band. Although these devices typically have short ranges because of heavy attenuation by physical barriers, weather, and atmospheric absorption, they provide high-range resolution resulting from the wide bandwidth. Typical mmWave radar applications include autonomous vehicles [Dokhanchi et al., 2019a], gesture recognition [Lien et al., 2016], cloud observation [Mishra et al., 2018], RF identification [Decarli et al., 2014], indoor localization [Mishra and Eldar, 2017b], and health monitoring [Fortino et al., 2012].

A recent rise of both radar and communications applications at terahertz (THz) band has also led to the development of integration of radar sensing and communications functionalities at these frequencies [Elbir et al., 2021]. The precise definition of THz band varies among different community members. Recent works in wireless communications generally define this band in the range 0.03–10 THz with an obvious overlap with the conventional mmWave frequencies. For the radar, microwave, and remote sensing engineers, THz band starts at the upper-mmWave limit of 100 GHz, and, in particular, low-THz term is used for the range 0.1–1 THz. In optics, on the other hand, THz spectrum is defined to end at 10 THz, beyond which frequencies are considered far-infrared. The Terahertz Technology and Applications Committee of the IEEE Microwave Theory and Techniques Society (MTT-S) focuses on the 0.3–3 THz range, while the IEEE Transactions on Terahertz Science and Technology Journal targets 0.3–10 THz.

Table 1.1 summarizes some of the co-existing communications services across various IEEE radar bands. In this chapter, we provide an overview of signal processing techniques and aspects of spectrum-sharing across different bands.

Table 1.1 Co-existing radar systems and communications services at different IEEE radar bands

IEEE radar band	VHF/UHF [30 MHz–1 GHz]	L [1–2 GHz]	S [2–4 GHz]	C [4–8 GHz]	X [8–12 GHz]	Ku, K, Ka, V, W, THz [12–300 GHz]
Example radar systems	FOPEN	ARSR	ASR, Next-Generation Weather Radar (NEXRAD)	TDWR	Mobile weather radars	Automotive radars, cloud radars
Co-existing communications	TV/broadcast/ 802.11ah/f	WiMAX, Joint Tactical Information Distribution System (JTIDS)	LTE	802.11a/ac	LTE	802.11ad, mmWave and THz communications

1.2 Policy and Licensing Issues

In the United States, a 75 MHz bandwidth within the 5.9 GHz band (specifically ranging from 5.850 to 5.925 GHz) has been exclusively assigned to intelligent transportation systems (ITSs) and car safety purposes for the past two decades, employing the dedicated short-range communications (DSRCs) technology. However, due to the lack of advancements in the DSRC band and the exponential growth of Wi-Fi technology, the Federal Communications Commission (FCC) recently designated the lower 45 MHz (5.850–5.895 GHz) for unlicensed applications, such as Wi-Fi. Consequently, only the upper 30 MHz spectrum (5.895–5.925 GHz band) is presently allocated for dedicated usage by ITS technologies. While the FCC has reserved 30 MHz of spectrum for critical safety services, advanced connected vehicle services will necessitate additional spectrum resources, particularly for data-intensive applications like augmented reality. Fortunately, the FCC has made available the 5 GHz unlicensed frequency band (~500 MHz) for 3GPP technologies, which can be utilized by cellular vehicle-to-everything (C-V2X) communications.

DSRC is an ad hoc communication system that operates independently of network infrastructure. Due to its widespread availability, many automobile manufacturers seeking to adopt V2X communications have favored the IEEE 802.11p standard, which serves as the foundation for DSRC. However, the implementation of 802.11p (and its successor, 802.11bd) necessitates the installation of numerous new access points (APs) and gateways, resulting in extended deployment time and increased costs. Given the absence of a clear business model, it is challenging to find an operator willing to bear the expenses associated with deploying numerous new APs based on freely available 802.11p/bd technologies. Consequently, the FCC has endorsed and prioritized C-V2X technologies based on the 3GPP standards, utilizing the 5.9 GHz frequency band, to pave the way for future connected vehicular systems. This includes requirements for over-the-air (OTA) software updates and the establishment of a car-to-cloud ecosystem.

The CBRS band serves as an intriguing case study due to the unequal access priority and the necessity of accurately detecting incumbents with 99% accuracy, even in the presence of lower-priority transmissions. Presently, tier 1 naval radar is safeguarded by a threshold limit on the combined power of noise and transmissions within the designated surrounding whisper zones. This necessitates a reduction in transmission power levels for LTE/5G priority access license (PAL) grantees, which consequently impacts consumer devices. The requirement for low power usage by PAL users becomes further complicated in the context of mobile radar, as the whisper zones may dynamically shift around the radar's moving location.

At higher frequencies, mmWave is generally considered to be unlicensed, depending on the jurisdiction. International Telecommunications Union (ITU) has completed guidelines for allocation of spectrum up to 275 GHz, and active discussions are currently underway to allot spectrum beyond 275 GHz.

1.3 Legal Challenges

Recent developments in spectrum-sharing allocation policies have highlighted the challenges that arise from overly cautious and inefficient utilization. For instance, the adoption of an outdated terrain-agnostic propagation model in the FCC TV Band ruling has artificially restricted the reuse of TV bands in areas where it would not interfere with broadcast TV receivers. In a highly publicized dispute, the Federal Aviation Administration (FAA) and the airline industry opposed the allocation of the C-band for 5G service deployment. The FAA relied on theoretical propagation models to

suggest potential interference with airplane radar altimeters, while the FCC conducted extensive measurements over a five-year rule-making process to demonstrate that the interference between C-band 5G devices and altimeters would be negligible in practical scenarios. More recently, the FCC granted permission for indoor usage of the 6–7 GHz band for indoor Wi-Fi 7 through a centralized automatic frequency coordination (AFC) system. This system employs the location of Wi-Fi APs to predict interference to nearby microwave relay receivers, which are the primary users of the band. It dynamically assigns permissible channels to the APs. However, AT&T and other microwave relay tower operators filed a lawsuit against the FCC. According to AT&T, "The FCC has no plan to mitigate the interference when it inevitably occurs. Once millions of these new unlicensed devices are released and in use, it will be impracticable, if not impossible, for the FCC to identify and remove specific devices causing interference."

1.4 Agency-Driven Projects

Significant synergistic efforts are currently underway for efficient radio spectrum utilization by multiple entities. The National Science Foundation (NSF) has sponsored the Enhancing Access to the Radio Spectrum (EARS) project that brings together many different users for a flexible access to the spectrum [Bernhard et al., 2010]. A significant advancement is due to the Defense Advanced Research Projects Agency's (DARPA) Shared Spectrum Access for Radar and Communications (SSPARC) program focused on spectrum sharing for S-band military radars [Jacyna et al., 2016]. However, with new and emerging communications systems and novel radar applications such as next-generation automobiles and medical and health monitoring devices, the spectral congestion issues now extend far beyond classical communications and military radar. Realization of such emerging versatile systems requires a holistic approach from multiple perspectives such as physical layer transmission/reception, protocols, and inter-system coordination, among others.

The significance of wireless spectrum in the nation's pursuit of economic prosperity, infrastructure development, and national security cannot be overstated. Recent strategic plans, such as the "Electromagnetic Spectrum Superiority Strategy" released by the Department of Defense in late 2020 and the "Presidential Memorandum on Developing a Sustainable Spectrum Strategy for America's Future" from 2018, emphasize the need to utilize RF spectrum efficiently and effectively to fulfill current and future economic, national security, scientific, safety, and federal mission objectives. An important advancement in spectrum sharing within the sub-6 GHz band is the opening of the CBRS band, which presents significant opportunities for deploying 4G LTE and 5G networks in the desirable mid-band frequencies ranging from 3.55 to 3.7 GHz. However, utilizing these frequency bands requires adherence to certain conditions, including the implementation of an FCC-certified sensing architecture to protect federal incumbents such as ship-borne radar. Consequently, environmental sensing capability (ESC) sensors are employed to detect these signals and subsequently update the spectrum access server (SAS), which manages spectrum allocations.

Apart from EARS, NSF has recently expanded on spectrum-sharing efforts through a volley of programs: Spectrum and Wireless Innovation enabled by Future Technologies (SWIFT), Platforms for Advanced Wireless Research (PAWR), RF Data Factory, and Spectrum Innovation Center (SpectrumX), to name a few. In 2023, the US government released a presidential memorandum to establish a National Spectrum Strategy Implementation Plan (NSSIP) through the National Telecommunications and Information Administration (NTIA).

1.5 Channel Considerations

The characteristics of cmWave, mmWave, and THz channels differ significantly, necessitating careful considerations in system design and deployment. In this section, we will explore the channel considerations of various bands, highlighting their key features and implications for communication systems. Understanding these channel aspects is crucial for developing effective strategies to overcome challenges and harness the full potential of these frequency bands in wireless communication applications.

1.5.1 cmWave vs mmWave

Strong Attenuation Compared to sub-6 GHz transmissions envisaged in 5G, mmWave signals encounter a more complex propagation environment characterized by higher scattering, severe penetration losses, and lower diffraction. These losses result in mmWave communications links being near line-of-sight (LoS) with fewer non-line-of-sight (NLoS) clusters and smaller coverage areas. Similarly, lower diffraction results in poorer coverage around corners. High attenuation also implies that mmWave radars are useful only at short ranges and, as a result, multipath is a less severe problem.

High Path-Loss and Large Arrays Quite naturally, the mmWave signals suffer from higher path-loss for fixed transmitter (TX) and receiver (RX) gains. By the Friis transmission formula, compensating for these losses while keeping the same effective antenna aperture (or increasing the gain) imposes constraints on the transceiver hardware. Since the received power is contingent on the beams of the transmitter and receiver being oriented toward each other, the same aperture is accomplished by using steerable antenna arrays whose elements are spaced by at most half the wavelength ($\lambda/2$) of the transmitted signal to prevent undesirable grating lobes. This inter-element spacing varies between 0.5 and 5 mm for mmWave carriers. Such narrow spacings impact the choice of RF and intermediate frequency (IF) elements because they should fit in the limited space available, and precise mounting may be difficult in, for instance, vehicular platforms.

Wide Bandwidths The unlicensed, wide mmWave bandwidth enables higher data rates for communications as well as the range resolution in radar. In automotive radar, this ensures detection of distinct, informative micro-motions of targets such as pedestrians and cyclists [Duggal et al., 2020]. The mmWave receivers sampling at the Nyquist rate require expensive, high-rate analog-to-digital converters (ADCs). Large bandwidths also imply that the use of low-complexity algorithms in transmitter and receiver processing is critical [Dokhanchi et al., 2019a]. Further, mmWave channels are sparse in both time and angular dimensions – a property exploited for low-complexity, low-rate reconstruction using techniques such as compressed sensing [Mishra and Eldar, 2017b, 2019]. It is crucial to consider if relevant narrowband assumptions hold in a mmWave application; otherwise, the signal bandwidth is very broad with respect to the center frequency and the steering vectors become frequency-dependent.

Power Consumption The power consumption of an ADC increases linearly with the sampling frequency. At baseband, each full-resolution ADC consumes 15–795 mW at 36 MHz–1.8 GHz bandwidths. In addition, power consumed by other RF elements such as power amplifiers and data interface circuits in conjunction with the narrow spacing between antenna elements renders

it infeasible to utilize a separate RF-IF chain for each element. Thus, a feasible multi-antenna TX/RX structure and beamformers should be analog or hybrid (wherein the potential array gain is exploited without using a dedicated RF chain per antenna and phase shifter (PS)) [Méndez-Rial et al., 2016] because fully digital beamforming is infeasible.

Short Coherence Times The mmWave environments such as indoor and vehicular communications are highly variable with typical channel coherence times of nanoseconds [Rappaport et al., 2015]. The reliability and coverage of dynamic mmWave vehicular links are severely affected by the use of narrow beams. The intermittent blockage necessitates frequent beam re-alignment to maintain high data rates. Also, mmWave radar requires a wide Doppler range to detect both fast vehicles and slow pedestrians [Duggal et al., 2020]. Short coherence times impact the use of feedback and waveform adaptation in many joint radar-communication (JRC) designs, where the channel knowledge may be invalid or outdated when transmit waveform optimization takes place.

1.5.2 Toward THz Band

Compared to the mmWave channel, the THz channel exhibits certain unique characteristics (Figure 1.1). The JRC-specific challenges are listed below [Elbir et al., 2021].

Path Loss The THz channel experiences substantial path loss, approximately 120 dB/100 m at 0.6 THz. This path loss is primarily influenced by spreading loss and molecular absorption, which are more significant compared to mmWave frequencies. To compensate for the high path loss, a large number of antennas are deployed in a user-centric manner, allowing for beamforming gain that generates multiple beams toward communication users and radar targets.

Multipath In mmWave frequencies, both LoS and NLoS multipath components play significant roles. However, at THz frequencies, NLoS paths, especially in outdoor scenarios, are negligible. For instance, the first- and second-order reflected paths are attenuated by an average of 5 and 15 dB, respectively. Consequently, the THz channel is primarily characterized as LoS-dominant and NLoS-assisted. The THz JRC system can benefit from the presence of NLoS paths to enhance diversity, particularly in communication scenarios with low-resolution beamforming. Simultaneously, the insignificance of NLoS paths is advantageous for THz sensing/radar applications, where an explicit LoS path between the transmitter and the target is required.

Transmission Range THz systems have shorter transmission ranges compared to mmWave frequencies due to significant attenuation. In the THz JRC system, there is a trade-off between the requirement for long transmission distances, such as up to 200 m, for sensing applications and the need for shorter ranges, like 20 m, to achieve a data rate of 100 Gbps in communication tasks. Recent automotive radar applications have reported a transmission distance of up to 200 m with specific attenuation of approximately X dB/km over the 0.1–0.3 THz range, with a path loss of 4 dB. However, shorter distances are necessary for communication scenarios, such as around 20 m, to achieve a data rate of 100 Gbps.

Channel Sparsity The utilization of a large number of antennas and the predominance of LoS characteristics make the THz channels highly sparse in the angular domain. Compared to their millimeter-wave counterparts, THz channels exhibit a smaller angular spread, approximately 10–15° at 140 GHz, as opposed to 20–100° at 60 GHz. This sparsity can be leveraged to employ subarray models such as array-of-subarrays (AoSA) and group-of-subarrays (GoSA), which help

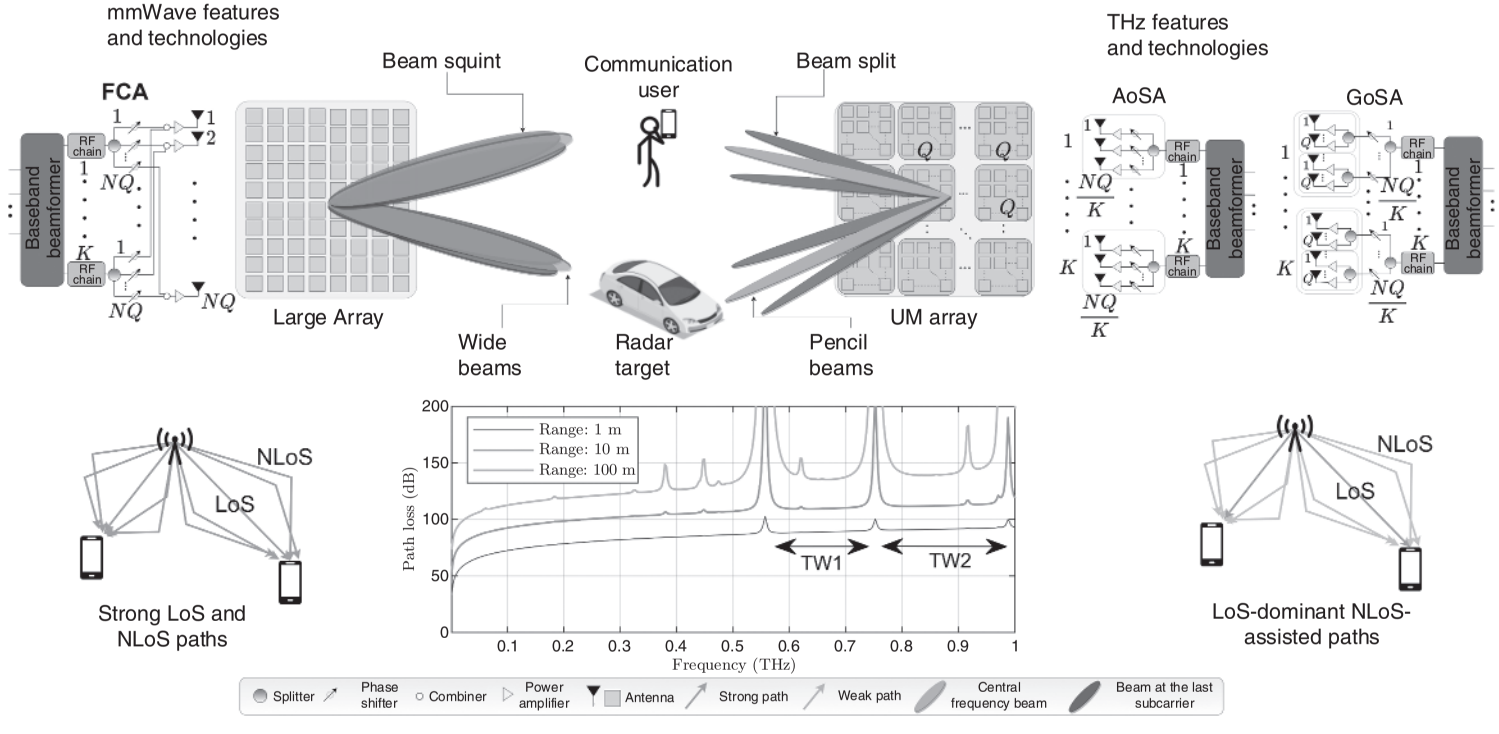

Figure 1.1 Comparison of millimeter-wave and THz band characteristics for JRC design including distance-dependent path loss, multipath components, beam alignment, and antenna array structures [Elbir et al., 2022].

reduce the hardware and computational complexities associated with high-frequency systems. Additionally, sparsity-based receivers can be designed to benefit both sensing and communication tasks in THz JRC systems.

Wideband Beam Split THz channels exhibit unique characteristics, including misalignment and phase uncertainties in PSs. The wideband mmWave systems commonly employ subcarrier-independent analog beamformers, but in THz channels, these beamformers can cause a phenomenon known as beam split. Due to the ultra-wide bandwidth, the generated beams split into different physical directions at each subcarrier. This effect, also referred to as beam squint in mmWave research, has more severe implications on achievable communication rates. In sensing applications, the beam split is approximately 4° (1.4°) for 0.3 THz with a bandwidth of 30 GHz (60 GHz with 2 GHz), respectively, for a broadside target direction-of-arrival (DoA).

Near-Field Effect Due to the shorter transmission distance in THz systems, the wave emitted from the transmitter and impinging on the receive array may no longer be a plane wave. In the near-field, specifically when the transmission range is shorter than the Fraunhofer distance, the wavefront becomes spherical. As a result, channel acquisition algorithms need to consider both direction and range information. While near-field signal processing is relatively new in the context of communication, it is a well-established concept in sensing/radar applications such as through-the-wall sensing, near-field imaging, and strip-map synthetic aperture radar (SAR). The range-dependent beampattern is also observed in certain far-field applications like frequency diverse array (FDA) radars, which use linear frequency offsets across antennas to achieve range-dependent beampatterns. However, the FDA wavefront is not spherical. Our focus is on the spherical wavefront near-field in a THz communication system that employs an extremely large array and transmits multiple subcarriers using orthogonal frequency-division multiplexing (OFDM) signaling.

Distance-Dependent Bandwidth In the low-THz band (below 1 THz), although there are regions of local attenuation minima, the frequency range exhibits distance-dependent spectral windows. While the entire band can be considered a single transmission window with a bandwidth on the order of a THz at distances below 1 m, at longer ranges, there are multiple transmission windows that are only tens or hundreds of GHz wide due to increased molecular absorption. The bandwidth of each transmission window decreases with range due to more severe absorption. For example, when the distance increases from 1 to 10 m, the bandwidth reduces by an order of magnitude. Therefore, in the THz band, there is a critical trade-off between operating radar or communication at high bandwidth and maintaining an adequate maximum detectable range or high data rates.

Doppler Shift In wideband THz systems, the Doppler spread can cause significant inter-carrier interference (ICI), especially in high mobility scenarios. At 0.3 THz, the Doppler shift becomes 10 times larger than that at 30 GHz. This severe Doppler effect undermines the orthogonality among subcarriers, leading to ICI and posing challenges for OFDM.

Table 1.2 summarizes the differences between the mmWave and THz channels.

Table 1.2 Comparison of mmWave and THz transmission characteristics [Elbir et al., 2022]

Phenomenon	mmWave	THz
Path loss	The path loss exponent ≈2. Massive array structures are used to mitigate path loss	The path loss exponent doubles. Ultra-massive arrays are employed to mitigate path loss
Channel model	Superposition of LoS and NLoS paths. Channel estimation may solely exploit sparse reconstruction techniques, e.g. compressed sensing (CS) and orthogonal matching pursuit (OMP)	A dominant LoS path with multiple NLoS paths. Channel estimation may require joint OMP and true-time-delay (TTD) techniques
Beam alignment	Beams are *squinted* but still cover the user across the entire bandwidth. This effect is largely dependent on the large number of antennas. Corrected via TTD processing at each antenna	Beams become totally *split* and cannot cover the user with their main lobes. This split is a function of both bandwidth and array size. Corrected by delay-phase precoding (DPP) or beam split phase correction
Array structure	Large arrays with fully-connected or subarray structures, where the latter has lower hardware complexity	Much larger array structures with additional subarray levels to reduce the hardware complexity, e.g. AoSA, widely spaced multi-subarray (WSMS) or GoSA structures
Bandwidth	Wideband throughout the entire range	Distance-dependent bandwidth arising from peculiarities in molecular absorption
Wavefronts	Planar wave in far-field	Spherical wavefront in near-field below Fraunhofer distance

We now present details of channel models commonly used in communications and radars.

1.5.3 Communications Channel

Consider a transmitter that employs an antenna array or a single directional antenna with carrier frequency f and TX (RX) antenna gain G_{TX} (G_{RX}). The LoS communications channel with a delay spread comprising $L_{\text{c}} - 1$ delay taps is $h_{\text{c}}(t,f) = G_{\text{c}} \sum_{\ell=0}^{L_{\text{c}}-1} \alpha_\ell \mathrm{e}^{-j2\pi\tau_\ell f} \mathrm{e}^{j2\pi\nu_\ell t}$, where G_{c} is the large-scale communications channel gain at the reception, and α_ℓ is the path loss coefficient of the l^{th} path with time delay τ_ℓ and Doppler shift ν_ℓ. The free space attenuation model yields $G_{\text{c}} = \frac{G_{\text{TX}} G_{\text{RX}} \lambda^2}{(4\pi)^2 \rho_{\text{c}}^\gamma}$, where γ is the path loss (PL) exponent. Further, $\gamma \approx 2$ for mmWave LoS outdoor urban [Rappaport et al., 2015] and rural scenarios [MacCartney et al., 2016].

1.5.4 Radar Channel

The doubly selective (time- and frequency-selective) mmWave radar channel is modeled after TX/RX beamforming using virtual representation obtained by uniformly sampling in the range dimension [Kumari et al., 2018]. Assume L uniformly sampled range bins and that the ℓth range bin consists of a few, (say) K_ℓ, virtual scattering centers. Each (ℓ, k)th virtual scattering center is characterized by its distance ρ_ℓ, delay τ_ℓ, velocity $v_{\ell,k}$, Doppler shift $\nu_{\ell,k} = 2v_{\ell,k}/\lambda$, large-scale

channel gain $G_{\ell,k}$, and small-scale fading gain $\beta_{\ell,k}$. Then, the multi-target radar channel model is $h_r(t,f) = \sum_{\ell=0}^{L-1} \sum_{k=0}^{K_\ell - 1} G_{\ell,k}\beta_{\ell,k} \mathrm{e}^{-j2\pi\tau_\ell f} \cdot \mathrm{e}^{-\mathrm{j}2\pi\nu_{\ell,k}t}$. The large-scale channel gain corresponding to the (ℓ, k)th virtual target scattering center is $G_{\ell,k} = \frac{\lambda^2\sigma_{\ell,k}}{64\pi^3\rho_\ell^4}$, where $\sigma_{\ell,k}$ is the corresponding scatterer's radar cross section (RCS). The small-scale gain is assumed to be a superposition of a complex Gaussian component and a fixed LoS component leading to Rician fading. Similarly, the corresponding frequency-selective models can also include Rician fading. They capture, as a special case, the spiky model used in prior works on mmWave communications/radar. In this case, the corresponding radar target models are approximated by the Swerling III/IV scatterers [Skolnik, 2008].

Further, clustered channel models can be considered to incorporate correlations and extended target scenarios although they remain unexamined in detail. For instance, the conventional mmWave automotive target model assumes a single non-fluctuating (i.e., constant RCS) scatterer based on the Swerling 0 model. This greatly simplifies the development and analysis of receive processing algorithms and tracking filters [Dokhanchi et al., 2019a]. However, when the target is located within the close range of high-resolution radar, the received signal is composed of multiple reflections from different parts of the same object. This *extended* target model is more appropriate for mmWave applications and may also include correlated RCS [Duggal et al., 2020].

It is typical to assume a frequency-selective Rayleigh fading model for both communications and radar channels during the dwell time comprising N_{CPI} coherent processing intervals (CPI). In radar terminology, this corresponds to Swerling I/II target models. In each CPI with M frames, the channel amplitude of each tap is considered to be constant, i.e., a block fading model is assumed. Moreover, constant velocity and quasi-stationarity conditions are imposed on the target model.

1.5.5 Channel-Sharing Topologies

The existing mmWave JRC systems could be classified by the joint use of the channel [Paul et al., 2017; Geng et al., 2018] (Figure 1.2). In the *spectral coexistence* approach, radar and communications operate as separate entities and focus on devising strategies to adjust transmit parameters and mitigate the interference adaptively for the other [Cohen et al., 2018]. To this end, some information exchange between the two systems, i.e. spectral cooperation, may be allowed but with minimal changes in the standardization, system hardware and processing. In *spectral co-design* [Dokhanchi et al., 2019a; Paul et al., 2017], new *joint* radio-frequency sensing and communications techniques are developed where a single unit is employed for both purposes while also accessing the spectrum in an opportunistic manner. New fully-adaptive, software-defined systems are attempting to integrate these systems into the same platform to minimize circuitry and maximize flexibility. Here, each transmitter and receiver may have multiple antennas in a phased array or Multiple-Input Multiple-Output (MIMO) configuration.

Some spectrum-sharing solutions also involve cooperation between radar and communications. The exchange of information, such as the channel state information (CSI), may also be facilitated via a fusion center [Li and Petropulu, 2017]. The spectral cooperation enables both systems to benefit from increased degrees of freedom (DoFs) and allows joint optimization of system parameters through one [He et al., 2019] or more [Dokhanchi et al., 2020] objective functions. Sometimes, sensing (communications) may be opportunistically present because of flexibility in the communications (radar) transmitter. Table 1.3 shows various other categories of JRC solutions. Apart from the abovementioned hardware-sharing criterion, it is possible to classify the JRC systems as follows:

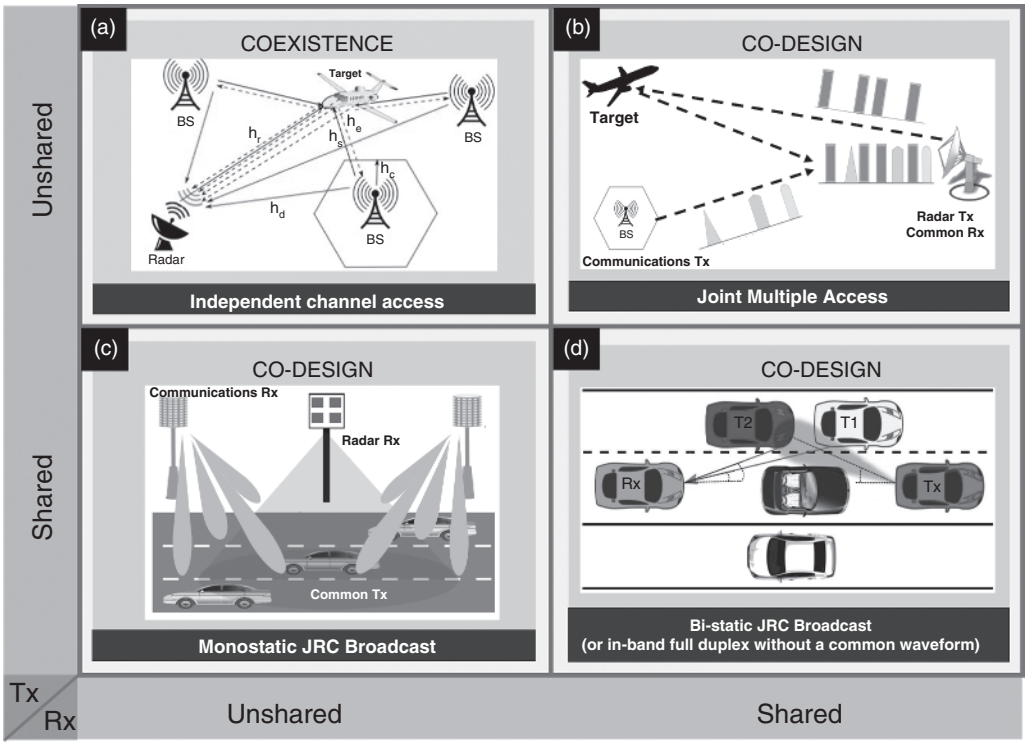

Figure 1.2 (a) Spectral coexistence system where radar and communications subsystems are independently located and access the associated radio channels such as radar target channel h_r, communications channel h_c, radar-to-communications interference h_s, and communications-to-radar interference h_d [Bică et al., 2016]. (b) Co-design system where only Rx are shared. In this *joint multiple access* channel, the radar operates in monostatic mode and both systems transmit different waveforms that are orthogonal in spectrum, code or time [Mishra et al., 2017]. (c) In TX-shared co-design, the monostatic radar functions as a communications transmitter emitting a common JRC waveform [Muns et al., 2019]. (d) A bi-static broadcast co-design with common TX, RX, and a joint waveform [Dokhanchi et al., 2019a]. The joint waveform transmitted by the TX vehicle bounces off from targets such as T1 and T2 and received by the Rx vehicle. A variant is an in-band full duplex system with different waveforms but common TX and Rx [Donnet and Longstaff, 2006]. The term "BS" stands for "base station."

Table 1.3 A comprehensive classification of JRC systems

Channel access	**Hardware**	**Waveform**
• Independent • Coordinated • Joint • Shared	• Separate Tx and Rx • Same Tx, Common Rx • Common Tx, Same Rx • Common Tx and Rx	• Separate • Common • Resource-shared
Location	**Performance/functionality**	**Specialized**
• Colocated • Bi-static • Distributed • Networked • Heterogeneous	• Radar-centric • Comms-centric • Joint radar-comms • Dual-Function Radar-Comms	• MRMC • IBFD ISAC • IRS-Aided ISAC • mmWave, THz, VLC, quantum

Channel Access Radar and communications systems may access channels independent of each other (as in spectral coexistence), jointly (as in spectral co-design), coordinating with each other as per requirements [Cohen et al., 2018], or on a fixed resource-shared basis [Alaee-Kerahroodi et al., 2019].

Waveforms Irrespective of whether the hardware is shared between radar and communications, both systems may employ separate waveforms [Cohen et al., 2018; Wu et al., 2022], a common waveform [Dokhanchi et al., 2019a], or the same waveform on a shared resource basis [Alaee-Kerahroodi et al., 2019].

Location When the radar transmitter and receiver are close to each other (or on a common platform), it is termed a monostatic or colocated JRC system [Dokhanchi et al., 2019b]. When the transmitter and receiver are on different platforms, e.g. in a vehicular environment described in Dokhanchi et al. [2019a], then the resulting system is termed bi-static. This is generalized to a distributed or multi-static JRC, which comprises multiple radar transmitters and receivers [Liu et al., 2020]. The multiple units may also be networked via fusion center [Li and Petropulu 2017]. In Wu et al. [2022], a heterogamous JRC system has been considered, where each radar is a different type of system (phased array, MIMO, or mechanically scanning).

Functionality In a selfish JRC paradigm, the overall architecture usually promotes the performance of only one system leading to radar-centric [Alaee-Kerahroodi et al., 2019; Wu et al., 2022] and communications-centric [Ayyar and Mishra, 2019] co-existence solutions. On the other hand, the holistic solution relies on extensive cooperation between the two systems in transmitting strategies and receiving processing [Wu et al., 2022]. This has also been termed as integrated sensing and communications (ISAC) system. A specific system is dual-function radar-communications (DFRC), which refers to any JRC system that employs the same hardware for radar or communications functions.

Specialized When both radar and communications are deployed in MIMO configuration with several transmit and receive antennas to benefit from high spectrum efficiency and spatial diversity, the resulting joint MIMO-radar-MIMO-communications (MRMC) systems are more challenging to optimize [Alaee-Kerahroodi et al., 2019; Liu et al., 2020]. Further, recent developments in massive MIMO utilize uplink/downlink (UL/DL) channel reciprocity via a vast number of service antennas to serve a lower number of mobile users with time-division duplexing. More recently, the MRMC systems have considered in-band full-duplexing (IBFD) communications that enable UL and DL to function in a single time/frequency channel through advanced self-interference cancellation techniques [Liu et al., 2020]. More recently, reconfigurable intelligent surface (RIS) or intelligent reflecting surfaces (IRS) [Hodge et al., 2023] have introduced unprecedented flexibility and adaptability toward smart wireless channels. Recent research [Wei et al., 2023a,b; Esmaeilbeig et al., 2024; Elbir et al., 2023] on JRC systems has demonstrated that RIS platforms enable enhanced signal quality, coverage, and link capacity. Finally, apart from mmWave and THz spectrum, sensing and communications have also been explored in the visible light [Fragner et al., 2022] and quantum regimes [Wang et al., 2022].

In the next section, we provide some examples of transmit and receive strategies for two major JRC topologies: coexistence and co-design.

1.6 JRC Coexistence

Interference management is central to spectral coexistence of different radio systems. This typically requires sensing the state of the shared spectrum and adjusting TX and RX parameters so that the impact of interference is sufficiently reduced and individual system performance is enhanced. We now present the figures of merit qualifying system performance and then discuss methodologies for coexistence.

1.6.1 Communications Performance Criteria

Since the goal of communications systems is to transfer data at a high rate error-free for a given bandwidth, the commonly used performance criteria include quality of service (QoS) indicators such as spectral efficiency, mutual information, channel capacity, pairwise error probability, bit/symbol error rates (BER/SER), and signal-to-interference-and-noise ratio (SINR). Given a communications signal model, the achievable spectral efficiency can be used as a universal communications performance criterion. In practice, the achievable spectral efficiency r is an upper bound, while the effective spectral efficiency r_{eff} depends on the implemented receiver (e.g. minimum mean square error or MMSE [Shi et al., 2004], decision feedback [Takizawa et al., 2012] or time-domain equalizer [Liu et al., 2013]), and is a fraction of the achievable spectral efficiency. The effective communications rate is then the product of the signal bandwidth W and r_{eff}.

1.6.2 Radar Performance Criteria

Radar systems, by virtue of their use in both detection and estimation, lend themselves to a plethora of performance criteria depending on the specific task. Target detection performance is characterized by probabilities of correct detection, mis-detection, and false alarm. In a parameter estimation task, mean square error (MSE) or variance in comparison to the Cramér-Rao Lower Bound (CRLB) is commonly considered. The CRLB defines the lower bound for estimation error variance for unbiased estimators. There are also several radar design parameters such as range/Doppler/angular resolution/coverage and the number of targets a radar can simultaneously resolve. In particular, the radar's ability to discriminate in both range and velocity is completely characterized by the *ambiguity function* (AF) of its transmit waveform; it is obtained by correlating the waveform with its Doppler-shifted and delayed replicas.

1.6.3 Interference Mitigation

The mmWave radar and communications TX and RX can use all of their DoFs such as different antennas, frequency, coding, transmission slots, power, or polarization to mitigate or avoid mutual interference. Interference may also be caused by leakage of signals from adjacent channels because of reusing identical frequencies in different locations. In general, the higher the frequency in mmWave bands, the weaker the multipath effects. The transmitters can adjust their parameters so that the level of interference is reduced at the receiver. To this end, awareness about the dynamic state of the radio spectrum and interference experienced in different locations, subbands, and time instances is desired. This may be in the form of feedback provided by the receivers to the transmitter about the channel response and SINR. Both the TX and RX can be optimized such that the SINR is maximized at the receivers for both subsystems.

1.6.3.1 Receiver Techniques

Interference mitigation may be performed only at the RX rendering CSI exchange optional. Typically, this requires multiple antenna at RX, a common feature at mmWave, and processing of the received signals in the spatial and/or temporal domain. These techniques employ receive array covariance matrix $\mathbf{m}\Sigma$ (or its estimate $\mathbf{m}\hat{\Sigma}$) in certain interference canceling RX structures. Here, the received signal space spanned by eigenvectors of $\mathbf{m}\Sigma$ is divided into two orthogonal subspaces of signal and interference-plus-noise. The received signal is then projected to a subspace orthogonal to the interference-and-noise subspace to enable processing of practically interference-free signals. If the interference impinges the receiver from angles different from the desired signal, RX beamforming is commonly used [Geng et al., 2018]. The beampattern design ensures high gains toward the desired signals and steers nulls toward the interference. Common solutions include Minimum Variance Distortionless Response (MVDR), Linearly Constrained Minimum Variance (LCMV), and diagonal loading [Vorobyov, 2014].

Advanced interference cancellation receivers estimate CSI, use feedback about channel response, or sense other properties of the state of the radio spectrum. These estimates are later used to cancel the interference contribution from the overall received signal. The coherence time of the channels should be sufficiently long that the feedback or channel estimates are not outdated during the interference cancellation process. These techniques either require knowledge of modulation schemes employed by coexisting radio systems or are applied to digital modulation methods only. A prime example is the Successive Interference Cancellation (SIC) method that decodes and subtracts the strongest signal first from the overall received signals and then repeats the same procedure by extracting the next weaker signal from the residual signal and so on [Paul et al., 2017]. In the absence of CSI, non-traditional radar interference models are used for robust communications signal decoders [Ayyar and Mishra, 2019].

1.6.3.2 Transmitter Techniques

Adapting transmitters and optimizing transmit waveforms may be used to minimize the impact of interferences in coexistence systems. In a considered coexistence scenario, for example, the optimization objective could be maximizing the SINR at each receiver while providing the desired data rate for each communications user and target Neyman-Pearson detector performance for radar users. Designing a precoder for each transmitter or/and decoders for each receiver achieves this goal by steering the interferences to a different space than the desired a signals.

One such example design in the context of MIMO communications and MIMO radar is the Switched Small Singular Value Space Projection (SSSVSP) method [Mahal et al., 2017] in which the interference is steered to space spanned by singular vectors corresponding to zero or negligible singular values. This method requires information exchange between the radar subsystem and communications base-stations. Another example of a precoder-decoder design for interference management in radar-communications coexistence is via Interference Alignment (IA) [Cui et al., 2018] where IA coordinates coexisting multiple transmitters such that their mutual interference aligns at the receivers and occupies only a portion of the signal space. The interference-free signal space is then used for radar and communications purposes.

1.7 JRC Co-Design

Central toward facilitating the co-design of radar and communications systems are waveform design and their optimization exploiting available DoFs (spatial, temporal, spectral, polarization). The optimization is based on the system performance criteria and availability of channel state

information (CSI), awareness about target scene, and the levels of unintentional or intentional interference at the receivers.

1.7.1 JRC Performance Criteria

In co-design, JRC waveforms are modeled to simultaneously improve the functionalities of both subsystems with some quantifiable trade-off. In Bliss [2014], a radar round-trip delay estimation rate is developed and coupled with the communications information rate. This radar estimation, however, is not drawn from the same class of distributions as that of communications data symbols and, therefore, provides only an approximate representation of the radar performance. However, potential invalidity of some assumptions limits the extension of this to estimation of other target parameters.

The mmWave designs in Kumari et al. [2017, 2020] for single- and multiple-target scenarios suggest an interesting JRC performance criterion that attempts to parallel the radar CRLB performance with a new effective communications symbol MMSE criteria as a function of effective maximum achievable communications spectral efficiency, r_{eff}. The MMSE communications criteria here is analogous to the mean-squared error distortion in the rate distortion theory. Let MMSE_{c} be the MMSE of a communications system with spectral efficiency r. Then MMSE_{c} and r are related to each other through the equation $\frac{1}{N}\text{Tr}\left[\log_2 \text{MMSE}_{\text{c}}\right] = -r$, where N is the code length. Therefore, the effective communications distortion MMSE (DMSE) that satisfies $\frac{1}{N}\text{Tr}\left[\log_2 \text{DMSE}_{\text{eff}}\right] = -r_{\text{eff}} = -\delta \cdot r$ can be defined as $\text{DMSE}_{\text{eff}} \triangleq \text{MMSE}_{\text{c}}^{\delta}$, where δ is a constant fraction of communications symbols transmitted in a CPI with the channel capacity C. The performance trade-off between communications and radar is quantified in terms of a weighted combination of the scalar quantities $\frac{1}{N}\text{Tr}\left[\log_2 \text{DMSE}_{\text{eff}}\right]$ and $\frac{1}{Q}\text{Tr}\left[\log_2 \text{CRLB}\right]$, respectively, where the log-scale is used to achieve proportional fairness between the communications distortion and radar CRLB values and Q is the number of detected targets. Pareto-optimal solutions that assign weights to different design goals have also been explored in this context [Ciuonzo et al., 2015].

Mutual information (MI) is also a popular waveform optimization criterion. At the radar receiver, depending on whether the communications signal reflected off the target is treated as useful energy or interference or ignored altogether, a different MI-based criterion results [Bică et al., 2016]. Although MI maximization enhances the characterizing capacity of a radar system, it does not maximize the probability of detection. The optimal radar signals for target characterization and detection tasks are generally different [Bică et al., 2016; Cohen et al., 2018].

1.7.2 Radar-Centric Waveform Design

We first consider the appropriate radar-centric waveforms here. These range from conventional signals to emerging multi-carrier waveforms.

Conventional Continuous Wave and Modulated Waveforms A simple continuous-wave (CW) radar provides information about only Doppler velocity. To extract range information, either the frequency/phase of the CW signal is modulated or very short duration pulses are transmitted. In practice, the well-known Frequency Modulated Continuous Wave (FMCW) and Phase Modulated Continuous Wave (PMCW) radars are used. A typical FMCW radar transmits one or multiple chirp signals wherein the frequency increases or decreases linearly in time and then the chirps reflected off the targets are captured at the receiver. Chirp bandwidth of a few GHz may be used to provide a range resolution of a few centimeters, e.g., a 4 GHz chirp achieves a range resolution of 3.75 cm. For

PMCW, binary pseudorandom sequences with desirable auto-correlation/cross-correlation properties are typically used. The AF of PMCW has lower sidelobes than FMCW, and PMCW is also easier to implement in hardware [Dokhanchi et al., 2019a].

A general bi-static, PMCW-JRC system using a uniform linear array (ULA) [Dokhanchi et al., 2019a] follows the topology shown in Figure 1.2d. The transmitter sends M repetitions of the PMCW code of length L from each of its N_t transmit antennas. The Doppler shift and flight time for the paths are assumed to be fixed over the CPI. The reflections from Q targets impinge on N_r receive antennas. Let t_c be chip time (time for transmitting one element of one PMCW code sequence, i.e., fast time). The Doppler shifts and the flight time for every path are assumed to be fixed over a coherent transmission time Mt_b, where $t_b = Lt_c$ is the time taken to transmit one block of code, i.e., slow time. The transmit waveform takes the form

$$x_i(t) = \sum_{m=0}^{M-1}\sum_{l=0}^{L-1} a_m e^{i\zeta_l} s\left(t - lt_c - mt_b\right) e^{j2\pi f_c t} e^{j(i-1)kd\ \sin\beta}, \tag{1.1}$$

where $i \in [1, N_t]$ and $a_m = e^{j\varphi_m}$ denote differential PSK symbols (DPSK) over slow time (time for sending one code sequence). The DPSK modulation is robust to constant phase shifts. Further, $s(t)$ is the elementary baseband pulse shape, $\zeta_l \in \{0, \pi\}$ is the binary phase code, $e^{j(n-1)kd\sin\beta}$ is the beam-steering weight for the nth antenna, $k = \frac{2\pi}{\lambda}$ is the wave number, and β is the angle between the radiating beam and the perpendicular to the ULA (for simplicity, we consider only azimuth and ignore common elevation angles). The transmitter steers the beam in multiple transmission from $\left[\frac{-\pi}{2}, \frac{\pi}{2}\right]$, each time with angle β. As shown in Figure 1.3, the communications and radar waveform for PMCW-JRC are combined in analog hardware.

Let $\Delta V_q^{(1)}$ be the radial relative velocity between the transmitter and the qth path, where superscript $(\cdot)^{(1)}$ refers to the transmitter-target path, and the corresponding Doppler shift is $f_{D_q}^{(1)} = \frac{\Delta V_q^{(1)}}{c} f_c$, where $c = 3 \times 10^8$ m/s is the speed of light. The signal impinging on the qth scatterer is

$$z_{q,n}(t) = \sum_{m=0}^{M-1}\sum_{l=0}^{L-1} h_{q,n}^{(1)} a_m e^{j\zeta_l} s\left(t - lt_c - mt_b - \tau_q^{(1)}\right) e^{j2\pi f_c t - j2\pi f_{D_q}^{(1)} t - j2\pi f_c \tau_q^{(1)}}, \tag{1.2}$$

where $\tau_q^{(1)}$ and $h_{q,n}^{(1)}$ are the qth point scatterer time delay and propagation loss for each path, respectively. We exploit the standard narrowband assumption to express the received signal as a phase-Doppler-shifted version of the transmit signal. Assume $\tau_q = \tau_q^{(1)} + \tau_q^{(2)}$ to be the total flight time corresponding to a bi-static range $R_q = c\tau_q$, where the superscript $(\cdot)^{(2)}$ denotes variable dependency on the target-receiver path. Assume $f_{D_q} = f_{D_q}^{(1)} + f_{D_q}^{(2)}$ to be the bi-static Doppler shift, and ψ_q to be the angle between the qth scatterer and the perpendicular line to receive ULA. After TX/RX beamforming and frequency synchronization, the received signal at antenna p, obtained as a superposition of these reflections, takes the form

$$\begin{aligned}
\tilde{y}_p(t) &= \sum_{q=1}^{Q}\sum_{n=1}^{N_t} h_{q,p}^{(2)} z_{q,n}\left(t - \tau_q^{(2)}\right) e^{j2\pi f_{D_q}^{(2)} t} + \tilde{N}_p(t) \\
&= \sum_{q=1}^{Q}\sum_{n=1}^{N_t}\sum_{m=0}^{M-1}\sum_{l=0}^{L-1} h_{q,p}^{(2)} h_{q,n}^{(1)} a_m e^{j\zeta_l} s\left(t - lt_c - mt_b - \tau_q^{(1)} - \tau_q^{(2)}\right) \\
&\quad \times e^{j2\pi\left(f_c - f_{D_q}^{(1)} - f_{D_q}^{(2)}\right)t} e^{j\eta_q} e^{-jkd\sin(\psi_q)(p-1)} + \tilde{N}_p(t),
\end{aligned} \tag{1.3}$$

where $e^{j\eta_q} = e^{-j2\pi\left(f_c\left(\tau_q^{(1)} + \tau_q^{(2)}\right) + \tau_{D_q}^{(1)}\tau_q^{(2)}\right)}$ is a static phase shift, $h_{q,p}^{(2)}$ accumulates the effect of the qth transmitter-target-receiver point scatterer, path-loss, and RCS of the target, and $\tilde{N}_p(t)$ is complex circularly symmetric white Gaussian noise with variance σ^2. An extended target is modeled as a

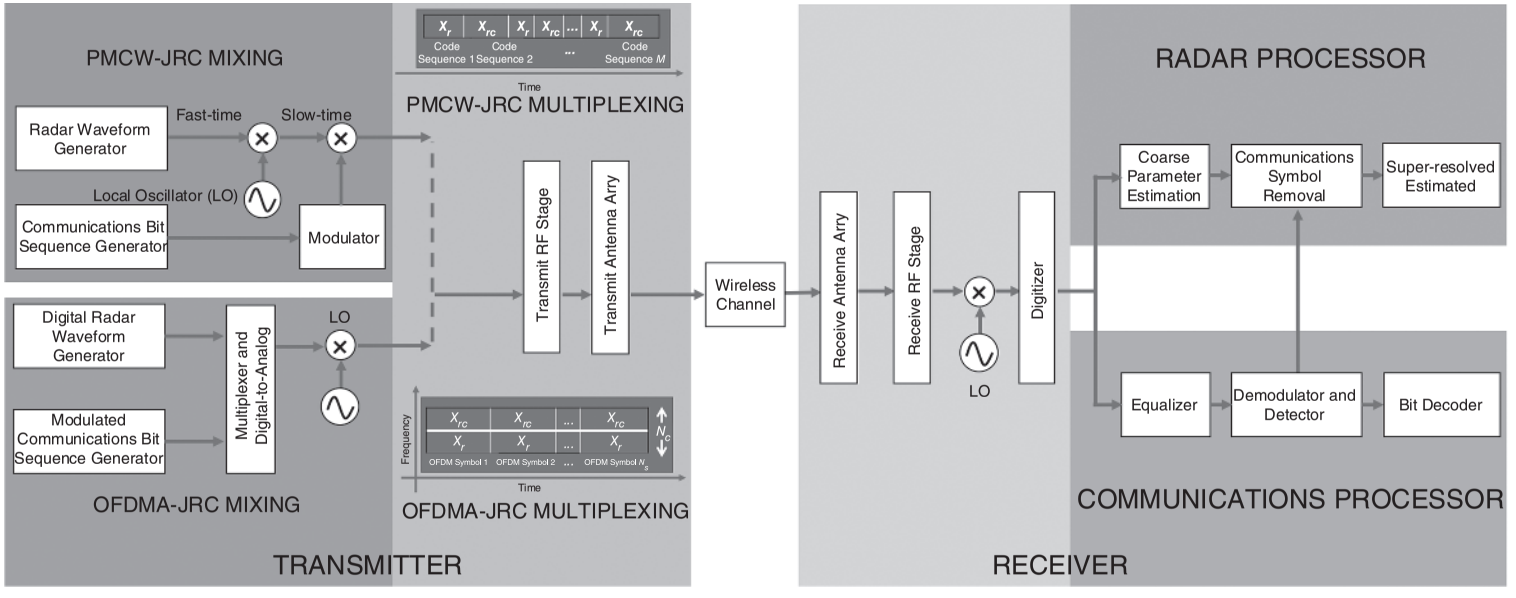

Figure 1.3 A simplified block diagram showing major steps of transmit and receive processing for a general mmWave JRC system. In the case of PMCW-JRC, the radar and communications waveforms are combined in the analog hardware before the RF stage. On the other hand, the information bits from these two subsystems are mixed digitally in OFDMA-JRC. The multiplexing of the radar-only and radar-communications frame for both PMCW- and OFDMA-JRC are depicted in the transmit portion. The receive processing for both systems is largely similar.

cluster of points. This combined with the superposition of reflections from the independent scatterer renders the model in (1.3) applicable for extended targets. After downconversion to baseband and ignoring RCS dependency on Tx and Rx antennas, i.e., $\sum_{n=1}^{N_t} h_{q,n}^{(1)} h_{q,p}^{(2)} e^{j\eta_q} = \sum_{n=1}^{N_t} d'_{q,p,n} = N_t d'_q = d_q$, the received signal is

$$y_p(t) = \sum_{q=1}^{Q} \sum_{m=0}^{M-1} \sum_{l=0}^{L-1} d_q a_m e^{-j2\pi f_{D_q} t} c_q^{p-1} e^{j\zeta_l} s\left(t - lt_c - mt_b - \tau_q\right) + N_p(t),$$
$$p \in \left[1, N_r\right], \tag{1.4}$$

where $c_q = e^{-jkd\sin(\psi_q)}$. Collecting the Nyquist time samples for the antenna p and rearranging them accordingly to slow/fast-time, we form a matrix,

$$\boldsymbol{Y}_p^{\text{PMCW-JRC}} = \sum_{q=1}^{Q} c_q^{p-1} d_q \text{Diag}\{\boldsymbol{a}\} \left[\left(\boldsymbol{b}_q^T \odot \boldsymbol{s}^T \boldsymbol{P}_{k_q}\right) \otimes \boldsymbol{e}_q\right] + \boldsymbol{N}_p \in \mathbb{C}^{M \times L}, \tag{1.5}$$

where vectors $\boldsymbol{e}_q = \left[e^{j2\pi f_{D_q} mLt_c}\right]_{m=1}^{M}$ and $\boldsymbol{b}_q = \left[e^{j2\pi f_{D_q} lt_c}\right]_{l=1}^{L}$ collect Doppler samples in slow and fast time, respectively, $\boldsymbol{s} = \left[e^{j\zeta_l}\right]_{l=0}^{L}$ contains L chips of code sequence, and $\boldsymbol{P}_{k_q}$ is a cyclic permutation matrix for a shift of k_q as

$$\boldsymbol{P}_{k_q} = \begin{bmatrix} \mathbf{0}_{K_q \times L - K_q} & \mathbf{I}_{K_q \times K_q} \\ \mathbf{I}_{L-K_q \times L-K_q} & \mathbf{0}_{L-K_q \times K_q} \end{bmatrix} \in \mathbb{C}^{L \times L}, \tag{1.6}$$

where $k_q \in \{0, \cdots, L-1\}$ is determined by range of the qth scatterer. If there is no delay between transmitter and receiver for all paths, then $k_q = 0$ for all q and $\boldsymbol{P}_{k_q}$ becomes an identity matrix.

In a PMCW-JRC, the communications symbols and Doppler parameters are coupled, thus leading to a non-identifiable model. This is resolved by a multiplexing strategy through which unknown parameters in the received signal are uniquely identified. The PMCW-JRC adopts time-division multiplexing between radar-only ($\mathbf{m}X_r$) and joint radar-communications ($\mathbf{m}X_{rc}$) frames that are transmitted for μ and $(1-\mu)$ % of the CPI, respectively. The value of μ depends on the amount of prior knowledge about the target scene. As a case in point, when the scene is stationary such as driving a straight path on a highway, we may not need full sensing capacity and can scale up the allocated time appropriately for communications. A coarse estimate of radar target parameters (range, angle, and Doppler) is obtained from $\boldsymbol{Y}_p^{\text{PMCW-JRC}}$ of radar-only frames $\mathbf{m}X_r$ while communications symbols are extracted from the received signal samples of the $\mathbf{m}X_{rc}$ frame. After extracting communications symbols from $\mathbf{m}X_{rc}$, the residual signal is exploited for further improving the radar target estimates through low-complexity JRC super-resolution algorithms [Dokhanchi et al., 2019a].

Multi-Carrier Waveforms Multi-carrier waveform radars provide additional DoFs to deal with dense spectral use and demanding mmWave target scenarios like drones, low-observable objects, and a large number of moving vehicles in an automotive scenario. Different DoFs can be used in an agile manner to achieve optimal performance depending on the radar task, nature of targets, and state of the radio spectrum. A general drawback of multi-carrier radar waveforms is their time-varying envelope leading to an increased Peak-to-Average-Power-Ratio (PAPR) or Peak-to-Mean-Envelope-Power-Ratio (PMEPR), which makes it difficult to use the amplifiers efficiently when high transmit powers are needed. However, in mmWave radars, the transmit powers tend to be small and surveillance ranges are short. The PAPR reduction is achieved by not

allocating all subcarriers or by using appropriate coding/waveform design. Hence, the PAPR issue in mmWave may be less severe.

Multi-carrier Complementary Phase Coded (MCPC) waveform [Levanon, 2000], wherein each subcarrier is modulated by a pseudorandom code sequence of a specific length, is also a viable mmWave JRC candidate. The MCPC design exploits DoFs in the spectral and code domain. In a sense, it is related to OFDM because after each subcarrier is modulated by a code in the time-domain, the subcarriers remain orthogonal without ICI. If the subcarriers are uncoded, the waveform is exactly OFDM. The inter-carrier spacing in MCPC needs to accommodate the spreading of the signals in frequency due to phase codes such as Barker, P3, or P4 polyphase codes [Skolnik, 2008]. This is achieved by choosing the inter-carrier spacing to be the inverse of the chip duration. In OFDM, inter-carrier spacing is smaller. A Generalized Multi-carrier Radar (GMR) waveform devised in Bică and Koivunen [2014, 2016] subsumes most of the widely used radar waveforms such as pseudo random frequency hopping (FH), MCPC, OFDM, and linear step approximations of linear FM signals, as special cases. A matrix model of transmitter and receiver is developed for GMR that allows for defining the waveforms and codes, spreading in time and frequency domain, power allocations, and active subcarriers using a compact notation. Different waveforms are obtained by choosing the dimensions of the matrix model and filling in the entries appropriately. This approach allows for relaxing the perfect orthogonality requirement; this may lead to a better resolution of target delays and Doppler velocities at mmWave.

Spatial DoFs and Multiple Waveforms A few different solutions use the same waveform for both subsystems but make use of radar's spatial DoFs for communications symbols. For instance, in Hassanien et al. [2016], the radar array beampattern sidelobes are modulated by communications messages along user directions. In Hassanien et al. [2018a], the communications symbols are represented by different pairing of antennas and waveforms in a MIMO configuration. Spatial DoFs are also useful for adaptively canceling specific users. A joint beamforming method is suggested in Hassanien et al. [2018b] for a dual-function radar-communications (DFRC) that comprises MIMO radar and communications systems assuming full-duplex transmission. The downlink communications signal is embedded into the transmit radar waveform, and uplink communications takes place when the radar is in listening mode. This necessitates accurate synchronization among the subsystems. The technique utilizes spatial diversity by enforcing the spatial signature of the uplink signals to be orthogonal to the spatial steering vectors associated with the radar target returns. The receiver beamformer employs adaptive and non-adaptive strategies to separate the desired communications signal from echoes of targets, clutter, and noise even if they impinge the array from the same direction. Other solution paths consist of finding spatial filters to mitigate in-band MIMO communications interference through optimization of the sidelobe and cross-correlation levels in MIMO radar systems [Aittomäki and Koivunen, 2017; Li et al., 2016], exploiting co-array processing with multiple waveforms [Zhang et al., 2015] and designing precoders/decoders through interference alignment [Cui et al., 2017].

However, for mmWave JRC systems, the full-resolution ADCs at the baseband signal result in an unacceptably high power consumption. This makes it infeasible to utilize an RF chain for each antenna element, implying that the prevailing MIMO systems that employ fully digital beamforming are not practical for mmWave systems. Thus, the benefits of using multiple waveforms for spatial mitigation in mmWave JRC systems are yet to be carefully evaluated. Currently, a single data stream model that supports analog beamforming with frequency flat TX/RX beam steering vectors is more common [Kumari et al., 2018]. Use of large antenna arrays in mmWave suggests that a feasible JRC approach could be to simply partition the arrays for radar and communications functionalities [Mishra and Eldar, 2019].

1.7.3 Communications-Centric Waveform Design

The most popular communications signal for mmWave JRC is OFDM because it provides a stable performance in multipath fading and relatively simple synchronization [Donnet and Longstaff, 2006]. Also, frequency division in duplexing has an added advantage; unlike time-division duplexing, the former employs different bands for uplink and downlink so that the impact on the interference in radar systems is less severe. Some solutions [Donnet and Longstaff, 2006; Dokhanchi et al., 2019a] also employ the related Orthogonal Frequency Division Multiple Access (OFDMA) waveform for a JRC system. While the OFDM users are allocated on only the time domain, the OFDMA users can be differentiated by both time and frequency. The latter, therefore, provides DoFs in both temporal and spectral domains. Although OFDM-JRC offers high dynamic range and efficient receiver processing implementation based on fast Fourier transform (FFT), it requires additional processing to suppress high sidelobes in receiver processing and reduce PAPR. Further, the OFDM cyclic prefix (CP), used to transform the frequency selective channel to multiple frequency at channels leading to a simplified equalizer, may be a nuisance in the radar context. The CP may adversely affect the radar's ability to resolve ambiguities in radar ranging. Its length depends on the number of channels, particularly the maximum excess delay that the radar signal may experience (time difference between first and last received component of the signal). For radar applications, the CP duration should be equal to or longer than the total maximum signal travel time between the radar platform and target. Other communications waveforms proposed for mmWave automotive JRC include spread spectrum, noise-OFDM, and multiple encoded waveforms [Dokhanchi et al., 2019a]. We now examine mmWave OFDMA-JRC in detail.

OFDMA-JRC Consider the same bi-static scenario of Figure 1.2d that we earlier analyzed for the PMCW-JRC system. The OFDMA-JRC transmitter (Figure 1.3) sends N_s OFDM symbols from N_t transmit antennas, and reflections from Q targets impinge on N_r receive antennas. Assume that β is the angle of departure. The Doppler shift and flight time for the paths are assumed to be fixed over a CPI, i.e., $N_s T_{sym}$, where T_{sym} is the duration of one OFDM symbol and $a_{n,m}$ are multiplexed communications/radar DPSK on the nth carrier of the mth OFDM symbol. Let N_c be the number of subcarriers and Δf be the subcarriers spacing, then the joint transmit waveform in baseband neglecting the CP is

$$x_i(t) = \sum_{m=0}^{N_s-1}\sum_{n=0}^{N_c-1} a_{n,m} e^{j2\pi f_n t} e^{jk\sin(\beta)(i-1)\frac{\lambda}{2}} s\left(t - mT_{\text{sym}}\right), \tag{1.7}$$

where $s(t)$ is a rectangular pulse of the width T_{sym}, $i \in [1, N_t]$, n and m are frequency and time indices, respectively, and $f_n = n\Delta f = \frac{n}{T_{sym}}$ [Dokhanchi et al., 2019a]. The received signal at the pth receiver over a CPI is

$$\begin{aligned}\tilde{y}_p(t) = &\sum_{m=0}^{N_s-1}\sum_{q=1}^{Q}\sum_{n=0}^{N_c-1}\sum_{i=1}^{N_t} d_{q,i,p} a_{n,m} e^{j2\pi f_n\left(t-\tau_q\right)} e^{j2\pi f_{D_q} t} e^{jk\sin\left(\psi_q\right)(p-1)\frac{\lambda}{2}} \\ &\times s\left(t - mT_{sym} - \tau_q\right) + \tilde{N}_p(t),\end{aligned} \tag{1.8}$$

where $\tilde{N}_p(t)$ is the additive noise on antenna p. Similar to PMCW-JRC, $d_{q,i,p}$ denotes path-loss, phase-shift caused by carrier frequency and RCS of the target; $d_{q,i,p}$ is independent of the subcarrier index due to narrowband assumption. Similarly, the Doppler is assumed to be identical for all subcarriers given a small inter-carrier spacing. For notational convenience, we omit the noise in

the following. We sample (1.8) at intervals $t_s = \frac{1}{N_c \Delta f}$ as

$$\tilde{y}_p\left[t_s\right] = \sum_{m=0}^{N_s-1}\sum_{q=1}^{Q}\sum_{n=0}^{N_c-1} d_q s_{n,m} e^{j2\pi\frac{nl}{N_c}} s\left(lt_s - mT_{\text{sym}} - \tau_q\right), \tag{1.9}$$

where $l \in [1, L]$, $n \in [1, N_c]$, and $L \leq N_c$, $d_q = \sum_{i=1}^{N_t} d_{q,i,p}$ as before, and $\tilde{s}_{n,m} = a_{n,m} e^{-j2\pi n\Delta f \frac{R_q}{c}} e^{j2\pi m T_{\text{sym}} f_{D_q}} e^{j\pi \sin(\psi_q)(p-1)} \tilde{s}_{n,m}$ contains information about range, Doppler, angle of arrival, and communications. We assume the number of inverse Fast Fourier Transform (IFFT) points N_c is equal to the number of fast-time samples L in each OFDM symbol. The received signal samples can be viewed as a radar data cube in spatial, spectral, and temporal domains with N_t antennas, N_c subcarriers, and N_s OFDM symbols. Let us stack the entire DPSK symbols into a matrix $\mathbf{m}A \in \mathbb{C}^{N_c \times N_s}$ and let $\mathbf{a}_m = [\mathbf{A}]_m$ be the communications symbols over all subcarriers at mth OFDM symbol time. For a given OFDM symbol, say m, collecting signals from all subcarriers across different antennas leads to the following slow-time slice of the data cube:

$$\mathbf{Y}_m^{\text{OFDMA-JRC}} = \mathbf{F}_{N_c} Diag\left(\mathbf{a}_m\right) \Xi\left(\frac{-\Delta f R_q}{c}\right) Diag\left(\boldsymbol{d}\right) \boldsymbol{C} \in \mathbb{C}^{N_c \times N_r}, m \in \left[1, N_s\right], \tag{1.10}$$

where $\Xi\left(\frac{-\Delta f R_q}{c}\right) = \left[e^{-j2\pi n\Delta f \frac{R_q}{c}}\right]_{n=1,q=1}^{N_c,Q} \in \mathbb{C}^{N_c \times Q}$, $\mathbf{C} = \left[e^{jk\sin(\psi_q)(p-1)\frac{\lambda}{2}}\right]_{q=1,p=1}^{Q,N_r}$, $\mathbf{C} \in \mathbb{C}^{Q \times N_r}$, and $\mathbf{d} = [d_1 \cdots d_Q]$. Further, $\mathbf{F}_{N_c} = \left[e^{j2\pi\frac{nl}{N_c}}\right]_{l=0,n=0}^{N_c-1,N_c-1}$ denotes a N_c-point IFFT matrix. To estimate Doppler shifts, we consider a subcarrier slice of data cube (1.9):

$$\mathbf{Z}_n^{\text{OFDMA-JRC}} = Diag\left(\mathbf{a}_n\right) \Xi\left(f_{D_q} T_{sym}\right) Diag\left(\mathbf{d}\right) \mathbf{C} \in \mathbb{C}^{N_s \times N_r}, \tag{1.11}$$

where $\mathbf{a}_n = [\mathbf{A}]_n \in \mathbb{C}^{N_s}$ are the DPSK symbols over slow time, $\Xi\left(f_{D_q} T_{sym}\right) = \left[e^{j2\pi m T_{sym} f_{D_q}}\right]_{m=1,q=1}^{N_s,Q}$.

As in PMCW-JRC, the receive processing of OFDMA-JRC is affected by coupling of communications symbols with a radar parameter (range in the case of OFDMA-JRC). To ensure that range estimation does not suffer by using all subcarriers, frequency-division multiplexing is employed in (1.2) such that μ% of the OFDMA subcarriers are allocated to radar (with known $a_{n,m}$ on these subcarriers) and the rest to JRC. The rest of the OFDMA-JRC receive processing is similar to PMCW-JRC (Figure 1.3) [Dokhanchi et al., 2019a].

Comparison of PMCW- and OFDMA-JRC While OFDMA encodes radar and communications simultaneously in the entire *time and space*, the PMCW does so in the entire *frequency and space*; hence, their DoFs and design spaces are in different domains. While it turns out that the receive system models of both waveforms are mathematically identical after matched filtering and retrieve all JRC parameters using similar super-resolution algorithms [Dokhanchi et al., 2017, 2019a], their individual performances mimic the respective communications and radar-centric properties. For example, the AF of the bi-static PMCW-JRC inherits the low sidelobes from its parent stand-alone PMCW radar waveform as shown in a comparison with the AF of OFDMA-JRC in Figure 1.4, given the same bandwidth. On the other hand, the PMCW-JRC is more sensitive to the number of users while the orthogonality of waveforms in OFDMA-JRC makes the latter robust to inter-channel interference. Finally, in a networked vehicle scenario, it requires less complex infrastructure and processing to apply PMCW with predefined or stored sequences rather than using OFDMA to adaptively allocate band to each user [Dokhanchi et al., 2019a; Donnet and Longstaff, 2006]. A comparison of estimation errors in the coupled parameter – range for OFDMA-JRC and Doppler for PMCW-JRC – using JRC super-resolution recovery [Dokhanchi et al., 2019a] is shown in Figure 1.5 for $\mu = 50\%$.

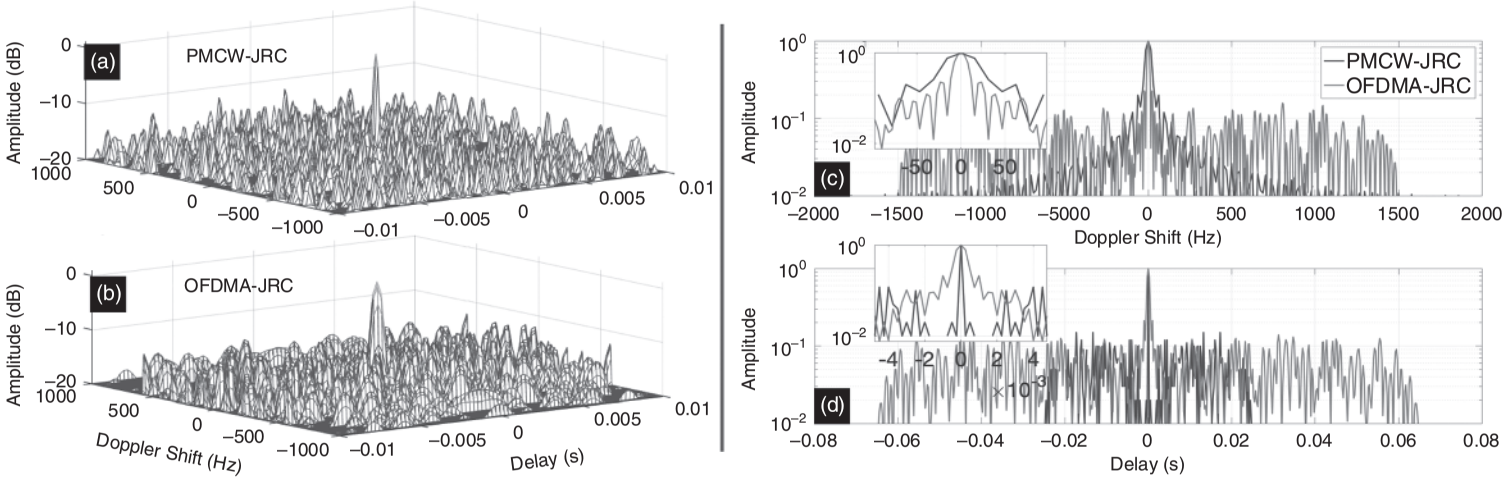

Figure 1.4 The AFs of bi-static mmWave JRC using (a) OFDMA and (b) PMCW signals with the (c) Doppler and (d) delay cuts [Dokhanchi et al., 2019a].

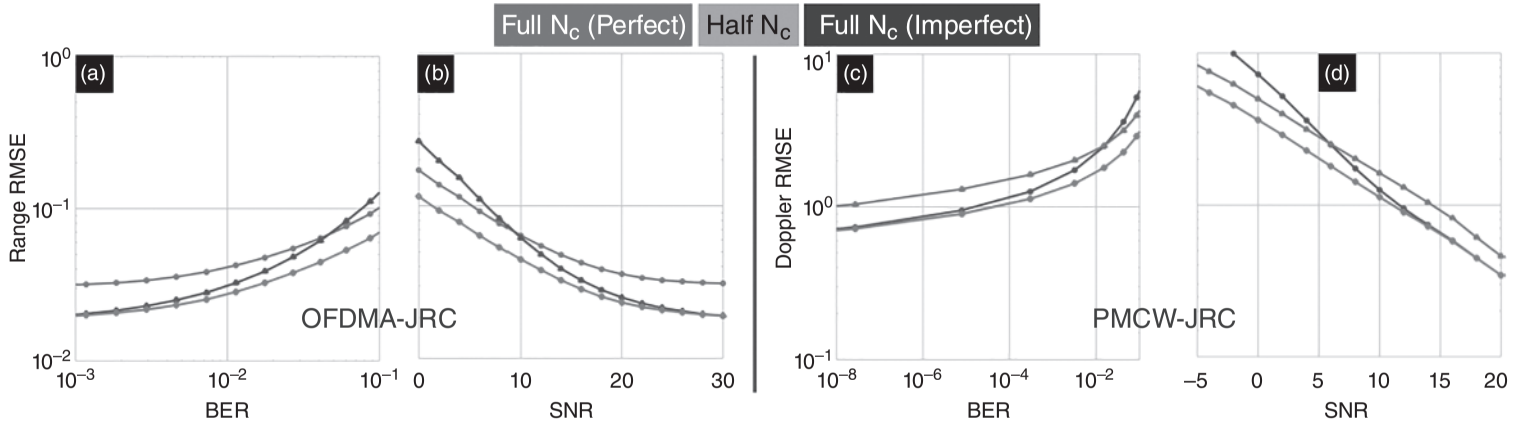

Figure 1.5 The root-mean-square-error (RMSE) of the estimated range of a single target using OFDMA-JRC with respect to (a) SNR and (b) BER using half (μ=50%) or all subcarriers (full N_c) with perfect and imperfect recovery of communications symbols. The RMSE in the Doppler estimate of a single target for PMCW-JRC using all and half frames with respect to (c) SNR and (d) BER. In both cases, JRC super-resolution algorithms [Dokhanchi et al., 2019a] have been employed.

1.7.4 Joint Coding

Recently, existing mmWave communications protocols that are embedded with codes that exhibit favorable radar ambiguity functions have been garnering much attention for JRC. In particular, the 60 GHz IEEE 802.11ad wireless protocol has been employed with time-division multiplexing of a radar-only and radar-communications frame. In general, these designs have temporal DoF (for a monostatic radar case). The IEEE 802.11ad single-carrier physical layer (SCPHY) frame consists of a short training field (STF), a channel estimation field (CEF), header, data, and beamforming training field. The STF and CEF together form the SCPHY preamble. CEF contains two 512-point sequences $Gu_{512}[n]$ and $Gv_{512}[n]$, each containing a *Golay complementary pair* of length 256, $\{Gau_{256}, Gbu_{256}\}$ and $\{Gav_{256}, Gbv_{256}\}$, respectively. A Golay pair has two sequences, Ga_N and Gb_N, each of the same length N with entries ± 1, such that the sum of their *aperiodic* autocorrelation functions has a peak of $2N$ and zero sidelobes:

$$Ga_N[n] * Ga_N[-n] + Gb_N[n] * Gb_N[-n] = 2N\delta[n], \tag{1.12}$$

where * denotes linear convolution. This property is useful for channel estimation and target detection.

By exploiting the preamble of a single SCPHY frame for radar, the existing mmWave 802.11ad waveform simultaneously achieves a cm-level range resolution and a Gbps data rate [Kumari et al., 2020]. The limited velocity estimation performance of this waveform can be improved by using multiple fixed-length frames in which preambles are reserved for radar [Kumari et al., 2018]. While this increases the radar integration duration leading to more accurate velocity estimation, the total preamble duration is also prolonged, causing a significant degradation in the communications data rate [Kumari et al., 2017]. A joint coding scheme based on the use of sparsity-based techniques in the time domain can minimize this trade-off between communications and radar [Kumari et al., 2020]. Here, the frame lengths are varied such that their preambles (exploited as radar pulses) are placed in non-uniformly. These non-uniform pulses in a CPI are then used to construct a virtual block of several pulses, increasing the radar pulse integration time and enabling an enhanced velocity estimation performance. If the channel is sparse, the same can be achieved in the frequency-domain using sub-Nyquist processing [Mishra and Eldar, 2017b]. In Duggal et al., [2020], the wide bandwidth of mmWave is exploited using a Doppler-resilient 802.11ad link to obtain very high resolution profiles in range and Doppler with the ability to distinguish various automotive targets. Figure 1.6 shows distinct, detailed movements of each wheel of a car and body parts of a pedestrian as detected by an 802.11ad-based Doppler-resilient short-range radar.

1.7.5 Carrier Exploitation

Selecting active subcarriers and controlling their power levels or PAPR in an adaptive manner is also useful for interference management. Radar systems generally utilize an entire bandwidth to achieve high resolution. On the other hand, communications systems often allocate resource blocks of a certain number of subcarriers to each user based on the channel quality indicator (CQI) to satisfy their rate and system QoS requirements. Through feedback from the receivers, spectrum sensing, databases, or other sources, the transmitters of both systems can have information about occupancy of different subcarriers, instantaneous or desired SINR levels, channel gains, and power

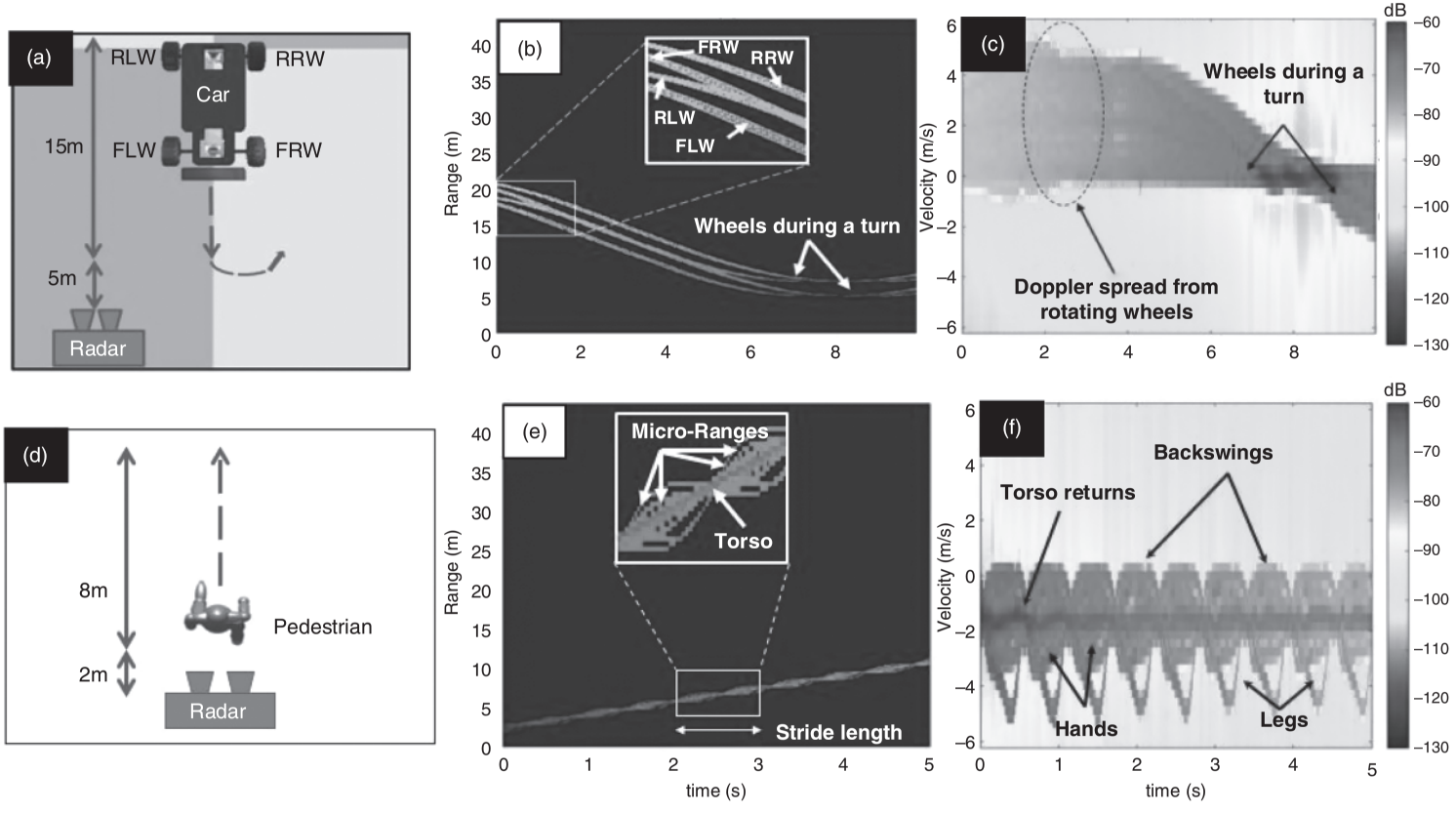

Figure 1.6 Radar signatures generated from animation models of (a) a small car and (d) a pedestrian using Doppler-resilient 802.11ad waveform [Duggal et al., 2019; Duggal et al., 2020]. As the targets move radially in front of the radar on the marked trajectories, the movements of the front right, front left, rear right, and rear left wheels (FRW, FLW, RRW, and LLW, respectively) of the car as well as the torso, arms, and legs of the pedestrian are individually observed in (b, e) range-time and (c, f) Doppler-time domains.

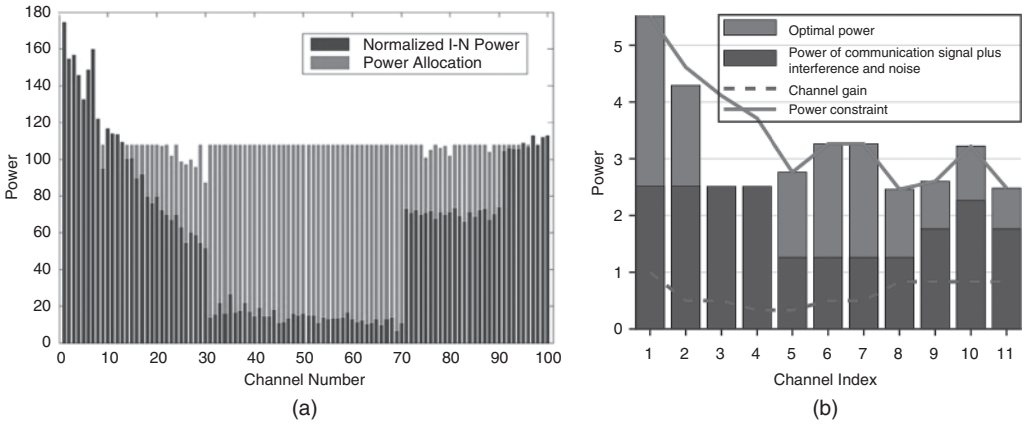

Figure 1.7 Power allocation solutions for JRC carrier exploitation via (a) water-filling and (b) Neyman-Pearson test [Bică et al., 2015].

constraints imposed by other coexisting subsystems. This awareness can be exploited in adaptively optimizing the power allocation among different subcarriers. An example of optimizing subcarrier power (P_k) allocations and imposing minimum desired rate constraints on wireless communications users and maximum power constraint P_{T} for the radar is as follows:

$$\begin{aligned} \underset{P_k,\eta}{\text{maximize}} \quad & p_{\mathrm{D}} \\ \text{subject to} \quad & p_{\mathrm{FA}} \leq \alpha, \\ & \log\left(1 + SINR_k\right) \geq t_k, \forall k, \\ & \sum_{k=0}^{N-1} P_k \leq P_{\mathrm{T}}, \end{aligned} \tag{1.13}$$

where η is the detection threshold for a likelihood ratio test using Neyman-Pearson detection strategy with false alarm constraint α. Two example power allocations from the radar perspective are depicted in Figure 1.7. A water-filling solution (Figure 1.7a) obtained by maximizing mutual information between received data and target and channel response allocates the radar power to those parts of spectrum where the signal experiences the least attenuation and the interference level is low. The second approach (Figure 1.7b) takes into account channel gains, required SINR values at communications subsystems while maximizing the radar performance in the Neyman-Pearson sense for the target detection task.

1.8 Emerging JRC Applications

Some more recent enabling architectures and technologies for JRC where the system can sense, learn, and adapt to the changes in the channel are as follows.

Cognitive Systems Cognitive radars and radios sense the spectrum and exchange information to build and learn their radio environment state. This typically implies channel estimation and feedback on channel quality. Spectrum cartography methods, which generate a map of spectrum access in different locations and frequencies at different time instances, have been developed in this context [Kim et al., 2011]. Based on the obtained awareness, operational parameters of

transmitters and receivers in each subsystem are adjusted to optimize their performance [Cohen et al., 2018]. Channel coherence times should be long enough for JRC to apply cognitive actions. Since this duration is in nanoseconds for mmWave environments, compressed sensing-based solutions aid in reducing the number of required samples for cognitive processing [Mishra and Eldar, 2017b,a].

Fast Waveforms Algorithms that develop cognitive waveforms should have low computational complexity in order to re-design waveforms on-the-fly, typically within a single CPI. This is especially important for mmWave systems where the fast-time radar waveform can easily have a length of tens of thousands of samples. In Li and Vorobyov [2018], waveform design in a spectrally dense environment does not exceed a quadratic complexity. In Mishra et al. [2017] and Mishra and Eldar [2017b], the mmWave radar based on sub-Nyquist sampling adaptively transmits in disjoint subbands, and the vacant slots are used by vehicular communications.

Machine Learning In order to facilitate fast configuration of mmWave JRC links with low latency and high efficiency, machine learning is useful to acquire situational awareness. This implies learning the evolution of spectrum state over time (including classifying radar target responses or other waveforms occupying the spectrum), acquiring the channel responses, identifying an underutilized spectrum, and exploiting it in an opportunistic manner. The deep learning methods are widely applied for tasks such as target classification, automatic waveform recognition, and determining optimal antennas and RF chains [Elbir and Mishra, 2019]. Optimal policies for coexisting systems may be learned using reinforcement learning approaches like the partially observable Markov decision process (POMDP) and the restless multi-arm bandit (RMAB) [Lunden et al., 2015].

Game Theoretic Solutions The interaction between radar and communications systems sharing a spectrum can be analyzed from a game theory perspective [Mishra et al., 2019]. The two systems or players form an adversarial, non-cooperative game because of conflicting interests in sharing the spectrum. The game is also dynamic due to continuously evolving spectral states over time. The utility function is designed to reflect the possible strategies based on the respective players' requirements. The solutions result in Nash or Stackelberg equilibrium, which are the game states with the property that none or one of the players can do better, respectively. In comparison to sub-6 GHz, the solution space for mmWave is several GHz wide with much lower maximum transmit power.

Resource Allocation A successful operation of spectrum-sharing systems relies on an efficient radio resource optimization [Wu et al., 2022]. In coexistence paradigms with a single antenna or fixed beamforming, the resources may include total transmit power, transmit signal bandwidth, and transmission time slots. Additionally, in phased array or MIMO systems, antennas need to be reserved for optimal sharing. In single-antenna JRC systems, the resource allocation objective is to optimize the transmit energy of the dual-purpose waveform based on the propagation channels of radar and communications users. In JRC systems that employ a transmit antenna array, highly directional beamforming toward the radar surveillance area while still ensuring sidelobes on the users offers an interesting solution. In JRC systems involving hybrid analog–digital transceiver architectures, antenna selection may also be viewed as a component of resource allocation objective.

Dual-Blind Deconvolution (DBD) In JRC systems, usually prior knowledge of the radar waveform and communications channel parameters is available. However, in applications such as covert and secure military systems, there is a need to decipher overlaid radar and communications signals with minimum prior information. Here, the primary objective shifts toward the simultaneous recovery of radar target parameters (e.g. delays, Doppler shifts), radar waveform, communications messages, and channel parameters. The radar transmit signal is also unknown in case of passive or multistatic sensing, where the transmitter and the receiver are separated platforms. Similarly, dynamic communications scenarios, like those found in mobile radio and vehicular networks, introduce a high level of channel dynamism, rendering prior channel estimates less accurate. In these cases of minimum prior information, recent works [Vargas et al., 2023; Monsalve et al., 2023; Jacome et al., 2023; Vargas et al., 2023] explored the low-rank structure of the waveforms and messages along with the sparsity of both radar and communications channels via atomic norm minimization. This framework facilitates the recovery of continuous-valued parameters, which is applicable to radar and communications channels. In Vargas et al. [2023], the recovery of both channels and signals is modeled as DBD, a highly ill-posed problem that is solved by minimizing the sum of multivariate atomic norms (SoMAN).

Tracking The presence of multiple targets in a distributed JRC scenario poses additional challenges. Compared to the well-studied single-target localization problems, one of the challenges involving multi-target localization using a widely distributed MIMO radar is as follows: since the relative distance of each target is different with respect to each receiver, the echoes from multiple targets are delayed by a different amount at each receiver. The result is that, after the detection procedure, each receiver ends up with a different ordering of targets in time. This makes it difficult to associate the detected echoes from all receiver uniquely to each target. To this end, the distributed JRC literature [Nayemuzzaman et al., 2024] suggests adapting various data association algorithms such as multiple hypothesis tracking, random finite sets, and joint probabilistic data association (JPDA) to assign detections correctly to each receiver. This technique paves way for integrating target tracking into distributed JRC scenarios.

1.9 Open Problems and Summary

In this chapter, we have explored the exciting field of JRC systems, which leverage the synergy between radar sensing and high-speed wireless communications. Throughout our discussion, we have identified several open problems that require further research and exploration to fully realize the potential of these integrated systems.

One of the key challenges is developing a correlation model between the sensing and communication channels. A quantitative description of the correlation between these channels is crucial for designing effective sensing-assisted communication schemes. Understanding the interplay between radar sensing and communication can enable the development of innovative techniques that exploit the shared information. These aspects need to be examined from both information theory and signal processing perspectives.

Coordination gain, which quantifies the benefits of JRC systems, requires further investigation. Developing accurate metrics and models to measure coordination gain will aid in evaluating the

performance of these integrated systems and guide their design and optimization. The literature either lacks a common design/performance metric or employs a vaguely defined common metric for both systems.

Another important aspect is the design of the JRC frame protocol. Developing unified JRC waveforms or beams that seamlessly integrate sensing and communication functionalities is a complex task. Designing efficient frame protocols that enable simultaneous sensing and communication while minimizing interference is an open problem that warrants further research.

Joint resource allocation, waveform design, and deployment/trajectory planning are critical for efficient operation of radar-communication systems. Optimizing the allocation of resources such as frequency, power, and time, as well as designing suitable waveforms and trajectories, can enhance system performance and enable seamless integration of radar and communications functionalities.

Coordinated interference management is another challenge that needs to be addressed. As radar and communications systems share the same spectrum, interference can arise between different users or even within the same user. Developing interference management techniques that effectively mitigate interference and enhance system performance is an important area for future research.

Cooperative JRC, where multiple radar-communication systems collaborate to achieve common goals, is an interesting avenue that requires further exploration. Investigating cooperative strategies, such as joint beamforming, resource sharing, and coordinated sensing, can lead to significant performance improvements and enhanced system robustness.

Integrating intelligent algorithms and techniques, such as artificial intelligence (AI), into emerging platforms like unmanned aerial vehicles (UAVs) holds great promise for JRC research. AI-based algorithms for UAV-aided JRC can enable autonomous decision-making, adaptive resource allocation, and optimized system performance.

Security and privacy are critical concerns in JRC systems. Developing secure JRC protocols that protect against eavesdropping, jamming, and other malicious activities is crucial for ensuring the confidentiality and integrity of the transmitted information [Mishra et al., 2022].

In conclusion, JRC is a vibrant and rapidly evolving area of research. Addressing the open problems discussed in this chapter will pave the way for the development of efficient, robust, and secure integrated systems. Continued research and innovation in these areas will enable the realization of the full potential of JRC systems in various applications, ranging from autonomous vehicles and smart cities to IoT and beyond [Sedighi et al., 2021].

References

Report to the President: Realizing the full potential of government-held spectrum to spur economic growth, 2012. President's Council of Advisors on Science and Technology.

T. Aittomäki and V. Koivunen. Hybrid optimization method for cognitive and MIMO radar code design. In *European Signal Processing Conference*, pages 2226–2229, 2017.

M. Alaee-Kerahroodi, K. V. Mishra, M. R. Bhavani Shankar, and B. Ottersten. Discrete phase sequence design for coexistence of MIMO radar and MIMO communications. In *IEEE International Workshop on Signal Processing Advances in Wireless Communications*, pages 1–5, 2019.

A. Ayyar and K. V. Mishra. Robust communications-centric coexistence for turbo-coded OFDM with non-traditional radar interference models. In *2019 IEEE Radar Conference (RadarConf)*, pages 1–6, 2019.

J. Bernhard, J. Reed, J. M. Park, A. Clegg, A. Weisshaar, and A. Abouzeid. Final report of the National Science Foundation workshop on Enhancing Access to the Radio Spectrum (EARS). *National Science Foundation*, Arlington, Virginia, Tech. Rep., 2010.

M. Bică and V. Koivunen. Frequency agile generalized multicarrier radar. In *Annual Conference of Information Sciences Systems*, 2014.

M. Bică and V. Koivunen. Generalized multicarrier radar: Models and performance. *IEEE Transactions on Signal Processing*, 64(17), 2016.

M. Bică, K. Huang, U. Mitra, and V. Koivunen. Opportunistic radar waveform design in joint radar and cellular communication systems. In *IEEE Global Communications Conference*, pages 1–7, 2015.

M. Bică, K. Huang, V. Koivunen, and U. Mitra. Mutual information based radar waveform design for joint radar and cellular communication systems. In *IEEE International Conference on Acoustics Speech and Signal Processing*, pages 3671–3675, 2016.

D. W. Bliss. Cooperative radar and communications signaling: The estimation and information theory odd couple. In *IEEE Radar Conference*, pages 50–55, 2014.

D. Ciuonzo, A. De Maio, G. Foglia, and M. Piezzo. Pareto-theory for enabling covert intrapulse radar-embedded communications. In *IEEE Radar Conference*, pages 0292–0297, 2015.

D. Cohen, K. V. Mishra, and Y. C. Eldar. Spectrum sharing radar: Coexistence via Xampling. *IEEE Transactions on Aerospace and Electronic Systems*, 29:1279–1296, 2018.

Y. Cui, V. Koivunen, and X. Jing. Interference alignment based precoder-decoder design for radar-communication co-existence. In *Asilomar Conference on Signals Systems and Computing*, pages 1290–1295, 2017.

Y. Cui, V. Koivunen, and X. Jing. Interference alignment based spectrum sharing for mimo radar and communication systems. In *IEEE International Workshop on Signal Processing and Advanced Wireless Communications*, pages 1–5, 2018.

R. C. Daniels and R. W. Heath Jr. 60 GHz wireless communications: Emerging requirements and design recommendations. *IEEE Vehicular Technology Magazine*, 2(3), 2007.

N. Decarli, F. Guidi, and D. Dardari. A novel joint RFID and radar sensor network for passive localization: Design and performance bounds. *IEEE Journal of Selected Topics in Signal Processing*, 8(1):80–95, 2014.

S. H. Dokhanchi, M. R. Bhavani Shankar, Y. A. Nijsure, T. Stifter, S. Sedighi, and B. Ottersten. Joint automotive radar-communications waveform design. In *IEEE International Symposium on Personal, Indoor and Mobile Communications*, pages 1–7, 2017.

S. H. Dokhanchi, B. S. Mysore, K. V. Mishra, and B. Ottersten. A mmWave automotive joint radar-communications system. *IEEE Transactions on Aerospace and Electronic Systems*, 55(3):1241–1260, 2019a.

S. H. Dokhanchi, M. Alaee-Kerahroodi, B. S. Mysore R., and B. Ottersten. Mono-static automotive joint radar-communications system. In *2019 IEEE 30th Annual International Symposium on Personal, Indoor and Mobile Radio Communications (PIMRC)*, pages 1–6, 2019b.

S. H. Dokhanchi, M. R. Bhavani Shankar, K. V. Mishra, and B. Ottersten. Multi-constraint spectral co-design for colocated MIMO radar and MIMO communications. In *IEEE International Conference on Acoustics, Speech and Signal Processing*, pages 4567–4571, 2020.

B. J. Donnet and I. D. Longstaff. Combining MIMO radar with OFDM communications. In *IEEE Radar Conference*, 2006.

G. Duggal, S. S. Ram, and K. V. Mishra. Micro-Doppler and micro-range detection via Doppler-resilient 802.11ad-based vehicle-to-pedestrian radar. In *IEEE Radar Conference*, 2019. Prepress.

G. Duggal, S. Vishwakarma, K. V. Mishra, and S. S. Ram. Doppler-resilient 802.11ad-based ultrashort range automotive joint radar-communications system. *IEEE Transactions on Aerospace and Electronic Systems*, 56(5):4035–4048, Oct 2020. doi: 10.1109/TAES.2020.2990393.

A. M. Elbir and K. V. Mishra. Deep learning design for joint antenna selection and hybrid beamforming in massive MIMO. In *IEEE International Symposium on Antennas and Propagation*, 2019. Prepress.

A. M. Elbir, K. V. Mishra, and S. Chatzinotas. Terahertz-band joint ultra-massive MIMO radar-communications: model-based and model-free hybrid beamforming. *IEEE Journal of Selected Topics in Signal Processing*, 15(6):1468–1483, 2021.

A. M. Elbir, K. V. Mishra, S. Chatzinotas, and M. Bennis. Terahertz-band integrated sensing and communications: Challenges and opportunities. arXiv preprint arXiv:2208.01235, 2022.

A. M. Elbir, K. V. Mishra, M. R. Bhavani Shankar, and S. Chatzinotas. The rise of intelligent reflecting surfaces in integrated sensing and communications paradigms. *IEEE Network*, 1–8, 2023.

T. Esmaeilbeig, K. V. Mishra, and M. Soltanalian. Beyond diagonal RIS: Key to next-generation integrated sensing and communications? arXiv preprint arXiv:2402.14157, 21 Feb 2024.

G. Fortino, M. Pathan, and G. Di Fatta. BodyCloud: Integration of cloud computing and body sensor networks. In *IEEE International Conference on Cloud Computing Technology and Science*, pages 851–856, 2012.

C. Fragner, A. P. Weiss, F. P. Wenzl, and E. Leitgeb. Integrated sensing and communication in the visible spectral range: A novel closed loop controller. In *2022 International Conference on Broadband Communications for Next Generation Networks and Multimedia Applications (CoBCom)*, pages 1–7, 2022.

Z. Geng, R. Xu, H. Deng, and B. Himed. Fusion of radar sensing and wireless communications by embedding communication signals into the radar transmit waveform. *IET Radar, Sonar and Navigation*, 12(6):632–640, 2018.

A. Hassanien, M. G. Amin, Y. D. Zhang, and F. Ahmad. Dual-function radar communication: Information embedding using sidelobe control and waveform diversity. *IEEE Transactions on Signal Processing*, 64(8):2168–2181, 2016.

A. Hassanien, M. G. Amin, Y. D. Zhang, and F. Ahmad. Signaling strategies for dual-function radar communications: An overview. *IEEE Aerospace and Electronic Systems Magazine*, 83(10):36–45, 2017.

A. Hassanien, E. Aboutanios, M. G. Amin, and G. A. Fabrizio. A dual-function MIMO radar-communication system via waveform permulation. *Digital Signal Processing*, 83:118–128, 2018a.

A. Hassanien, C. Sahin, J. Metcalf, and B. Himed. Uplink signaling and receive beamforming for dual-function radar communications. In *IEEE International Workshop on Signal Processing and Advanced Wireless Communications*, pages 1–5, 2018b.

Q. He, Z. Wang, J. Hu, and R. S. Blum. Performance gains from cooperative MIMO radar and MIMO communication systems. *IEEE Signal Processing Letters*, 26(1):194–198, 2019.

J. A. Hodge, K. V. Mishra, B. M. Sadler, and A. I. Zaghloul. Index-modulated metasurface transceiver design using reconfigurable intelligent surfaces for 6G wireless networks. *IEEE Journal of Selected Topics in Signal Processing*, 17(6):1248–1263, 2023.

R. Jacome, E. Vargas, K. V. Mishra, B. M. Sadler, and H. Arguello. Factor graph processing for dual-blind deconvolution at ISAC receiver. In *2023 IEEE 9th International Workshop on Computational Advances in Multi-Sensor Adaptive Processing (CAMSAP)*, pages 276–280, 2023.

G. M. Jacyna, B. Fell, and D. McLemore. A high-level overview of fundamental limits studies for the DARPA SSPARC program. In *IEEE Radar Conference*, pages 1–6, 2016.

S.-J. Kim, E. Dall'Anese, and G. B. Giannakis. Cooperative spectrum sensing for cognitive radios using Kriged Kalman filtering. *IEEE Journal of Selected Topics in Signal Processing*, 5(1):24–36, 2011.

P. Kumari, D. H. N. Nguyen, and R. W. Heath. Performance trade-off in an adaptive IEEE 802.11ad waveform design for a joint automotive radar and communication system. In *IEEE International Conference on Acoustics Speech and Signal Processing*, 2017.

P. Kumari, J. Choi, N. Gonzalez-Prelcic, and R. W. Heath Jr. IEEE 802.11ad-based radar: An approach to joint vehicular communication-radar system. *IEEE Transactions on Vehicular Technology*, 67(4):3012–3027, 2018.

P. Kumari, S. A. Vorobyov, and R. W. Heath. Adaptive virtual waveform design for millimeter-wave joint communication–radar. *IEEE Transactions on Signal Processing*, 68:715–730, 2020. doi: 10.1109/TSP.2019.2956689.

N. Levanon. Multifrequency radar signals. In *IEEE International Radar Conference*, pages 683–688, 2000.

B. Li and A. Petropulu. Joint transmit designs for co-existence of MIMO wireless communications and sparse sensing radars in clutter. *IEEE Transactions on Aerospace and Electronic Systems*, 53(6):2846–2864, 2017.

Y. Li and S. A. Vorobyov. Fast algorithms for designing multiple unimodular waveform(s) with good correlation properties. *IEEE Transactions on Signal Processing*, 66(5):1197–1212, 2018.

B. Li, A. P. Petropulu, and W. Trappe. Optimum co-design for spectrum sharing between matrix completion based MIMO radars and a MIMO communication system. *IEEE Transactions on Signal Processing*, 64(17):4562–4575, 2016.

J. Lien, N. Gillian, M. E. Karagozler, P. Amihood, C. Schwesig, E. Olson, H. Raja, and I. Poupyrev. Soli: Ubiquitous gesture sensing with millimeter wave radar. *ACM Transactions on Graphics*, 35(4):142:4–142:19, 2016.

W.-C. Liu, F.-C. Yeh, T.-C. Wei, C.-D. Chan, and S.-J. Jou. A digital Golay-MPIC time domain equalizer for SC/OFDM dual-modes at 60 GHz band. *IEEE Transactions on Circuits and Systems I: Regular Papers*, 60(10):2730–2739, 2013.

J. Liu, K. V. Mishra, and M. Saquib. Co-designing statistical MIMO radar and in-band full-duplex multi-user MIMO communications. arXiv preprint arXiv:2006.14774, 2020.

J. Lunden, V. Koivunen, and H. V. Poor. Spectrum exploration and exploitation for cognitive radio: Recent advances. *IEEE Signal Processing Magazine*, 32(3):123–140, 2015.

G. R. MacCartney, Jr., S. Sun, T. S. Rappaport, Y. Xing, H. Yan, J. Koka, R. Wang, and D. Yu. Millimeter wave wireless communications: New results for rural connectivity. In *ACM Workshop on All Things Cellular*, pages 31–36, 2016.

J. A. Mahal, A. Khawar, A. Abdelhadi, and T. C. Clancy. Spectral coexistence of MIMO radar and MIMO cellular system. *IEEE Transactions on Aerospace and Electronic Systems*, 53(2):655–668, 2017.

R. Méndez-Rial, C. Rusu, N. González-Prelcic, A. Alkhateeb, and R. W. Heath. Hybrid MIMO architectures for millimeter wave communications: Phase shifters or switches? *IEEE Access*, 4:247–267, 2016.

K. V. Mishra and Y. C. Eldar. Performance of time delay estimation in a cognitive radar. In *IEEE International Conference on Acoustics Speech and Signal Processing*, pages 3141–3145, 2017a.

K. V. Mishra and Y. C. Eldar. Sub-Nyquist channel estimation over IEEE 802.11ad link. In *IEEE International Conference on Sampling Theory and Applications*, pages 355–359, 2017b.

K. V. Mishra and Y. C. Eldar. Sub-Nyquist radar: Principles and prototypes. In A. De Maio, Y. C. Eldar, and A. Haimovich, editors, *Compressed sensing in radar signal processing*. Cambridge University Press, 2019. Prepress.

K. V. Mishra, A. Gharanjik, M. R. Bhavani Shankar, and B. Ottersten. Deep learning framework for precipitation retrievals from communication satellites. In *European Conference on Radar in Meteorology and Hydrology*, page 023, 2018.

K. V. Mishra, A. Zhitnikov, and Y. C. Eldar. Spectrum sharing solution for automotive radar. In *IEEE Vehicular Technology Conference – Spring*, pages 1–5, 2017.

K. V. Mishra, A. F. Martone, and A. I. Zaghloul. Power allocation games for overlaid radar and communications. In *URSI Asia-Pacific Radio Science Conference*, 2019. Prepress.

K. V. Mishra, A. Chattopadhyay, S. S. Acharjee, and A. P. Petropulu. OptM3Sec: Optimizing multicast IRS-aided multiantenna DFRC secrecy channel with multiple eavesdroppers. In *IEEE International Conference on Acoustics, Speech and Signal Processing (ICASSP)*, pages 9037–9041, 2022.

J. Monsalve, E. Vargas, K. V. Mishra, B. M. Sadler, and H. Arguello. Beurling-Selberg extremization for dual-blind deconvolution recovery in joint radar-communications. In *2023 IEEE 9th International Workshop on Computational Advances in Multi-Sensor Adaptive Processing (CAMSAP)*, pages 246–250, 2023.

G. R. Muns, K. V. Mishra, C. B. Guerra, Y. C. Eldar, and K. R. Chowdhury. Beam alignment and tracking for autonomous vehicular communication using IEEE 802.11ad-based radar. In *IEEE Infocom Workshops – Hot Topics in Social and Mobile Connected Smart Objects*, 2019. Prepress.

S. Nayemuzzaman, J. Liu, K. V. Mishra, and M. Saquib. Co-designing statistical MIMO radar and in-band full-duplex multi-user MIMO communications – Part III: Multi-target tracking. arXiv preprint arXiv, 2024.

B. Paul, A. R. Chiriyath, and D. W. Bliss. Survey of RF communications and sensing convergence research. *IEEE Access*, 5:252–270, 2017.

T. S. Rappaport, G. R. MacCartney, M. K. Samimi, and S. Sun. Wideband millimeter-wave propagation measurements and channel models for future wireless communication system design. *IEEE Transactions on Communications*, 63(9), 2015.

S. Sedighi, K. V. Mishra, M. R. Bhavani Shankar, and B. Ottersten. Localization with one-bit passive radars in narrowband Internet-of-Things using multivariate polynomial optimization. *IEEE Transactions on Signal Processing*, 69:2525–2540, 2021.

T. Shi, S. Zhou, and Y. Yao. Capacity of single carrier systems with frequency-domain equalization. In *IEEE Symposium on Circuits and Systems. Emerging Technology: Frontiers of Mobile Wireless Communication*, volume 2, pages 429–432, 2004.

M. I. Skolnik. *Radar handbook*. McGraw-Hill, third edition, 2008.

K. Takizawa, M. Kyrö, K. Haneda, H. Hagiwara, and P. Vainikainen. Performance evaluation of 60 GHz radio systems in hospital environments. In *IEEE International Conference on Communications*, pages 3219–3295, 2012.

E. Vargas, K. V. Mishra, R. Jacome, B. M. Sadler, and H. Arguello. Dual-blind deconvolution for overlaid radar-communications systems. *IEEE Journal on Selected Areas in Information Theory*, 4:75–93, 2023. doi: 10.1109/JSAIT.2023.3287823.

S. A. Vorobyov. Adaptive and robust beamforming. In A. M. Zoubir, M. Viberg, R. Chellappa, and S. Theodoridis, editors, *Array and statistical signal processing*, volume 3 of *Academic Press Library in Signal Processing*, pages 503–552. Academic Press, 2014.

S.-Y. Wang, T. Erdoğan, U. Pereg, and M. R. Bloch. Joint quantum communication and sensing. In *2022 IEEE Information Theory Workshop (ITW)*, pages 506–511, 2022.

T. Wei, L. Wu, K. V. Mishra, and M. R. Bhavani Shankar. Multi-IRS-aided Doppler-tolerant wideband DFRC system. *IEEE Transactions on Communications*, 71(11):6561–6577, 2023a.

T. Wei, L. Wu, K. V. Mishra, and B. Shankar. RIS-aided wideband holographic DFRC. *IEEE Transactions on Aerospace and Electronic Systems*, 2023b. doi: 10.1109/TAES.2024.3374272.

L. Wu, K. V. Mishra, M. R. Bhavani Shankar, and B. Ottersten. Resource allocation in heterogeneously-distributed joint radar-communications under asynchronous Bayesian tracking framework. *IEEE Journal on Selected Areas in Communications*, 40(7):2026–2042, July 2022.

W. Zhang, S. A. Vorobyov, and L. Guo. DOA estimation in MIMO radar with broken sensors by difference co-array processing. In *IEEE International Workshop on Computational Advances in Multi-Sensor Adaptive Processes*, 2015.